density of each band was quantified using the Scion Image Program (Scion Corporation, Frederick, MD, USA).

4.6. *Surgical procedure for gerbil forebrain ischemia*

Earlier studies found that hippocampal CA1 pyramidal cells are selectively vulnerable to ischemia and undergo apoptosis after transient ischemia (Kirino, 1982; Kirino and Sano, 1984). Gerbils were anesthetized with 2.5% isoflurane in 70% N_2O and 30% O_2. The common carotid arteries were exposed, and after completion of the surgical procedures, the isoflurane was discontinued. Then 1 min later both carotid arteries were occluded for 10 min using Sugita No. 51 temporary aneurysm clips (MIZUHO Co. Ltd., Tokyo, Japan). The body temperature of the animals was maintained at 36.5–37.0 °C using a heating pad with a heating lamp during the operation period and until a righting reflex reappeared. Sham-operated animals were treated in the same manner, except for the absence of occlusion.

4.7. *Immunohistochemistry*

At 7 days after the above ischemia, gerbils were anesthetized with sodium pentobarbital (Nembutal, 50 mg/kg, i.p.), and the brains were perfusion-fixed with 4% paraformaldehyde in 0.1 M phosphate buffer (pH 7.4). The brains were removed after a 20-min perfusion-fixation at 4 °C, and then immersed in the same fixative solution overnight at 4 °C. The brains were next immersed in 25% sucrose in 0.1 M phosphate buffer for 24 h, then frozen in powdered dry ice. Serial coronal sections 10 μm thick were cut on a cryostat at −20 °C, and stored at −80 °C until immunostaining.

Brain sections were rehydrated in phosphate-buffered saline (PBS), then treated with 0.3% hydrogen peroxidase in methanol. They were then washed three times in PBS, followed by pre-incubation with 10% normal goat serum. They were then incubated with primary antibodies overnight at 4 °C. Next, the slides were washed, then incubated with biotinylated anti-mouse IgG. They were subsequently incubated with avidin–biotin-peroxidase complex for 30 min, then developed using diamino benzidine peroxidase substrate.

4.8. *Histological analysis and detection of apoptosis*

Sections were stained with cresyl violet, and neuronal degeneration was quantified as described previously (Hara et al., 1990). The number of neurons per 1 mm linear length of the stratum pyramidale of the hippocampal CA1 subfield (neuronal density) was calculated by counting living neurons (using a microscope) and measuring the total length of the CA1 cell layer in each section. The average of the neuronal densities on the two sides was regarded as the neuronal cell density of each gerbil, according to the method of Kirino et al. (1986). The linear length of the CA1 subfield was measured using Image J (http://rsb.info.nih.gov/ij/download/). Apoptosis was detected by a TUNEL method using an *in situ* apoptosis detection kit.

4.9. *Intracerebroventricular injection*

Gerbils were anesthetized as described elsewhere (Oida et al., 2008), then mounted on a stereotaxic apparatus. Thereafter, anesthesia was maintained using 1.5% isoflurane. Five microliters of vehicle (10% DMSO in saline) or BIX (10 or 40 μg) was stereotaxically administered into the lateral ventricle over a period of 7 min, according to the atlas of Loskota et al. (1974). The site was 0.6 mm posterior to bregma, 1.2 mm lateral to the midline, and 2.0 mm below the dural surface. In sham-operated animals, the cannulation was made, but no injection (and no arterial occlusion; see below) was performed. Thirty minutes after the righting reflex had been regained, both common carotid arteries were exposed under 1.5% isoflurane anesthesia, then occluded bilaterally for 5 min as described above. The body temperature of the animals was maintained as described above. At 7 days after the ischemia, the effects of BIX on neuronal death were evaluated using cresyl violet-, NeuN-, and TUNEL-staining, as described above.

4.10. *Statistical analysis*

Data are presented as the means ± S.E. Statistical comparisons were made using a one-way ANOVA followed by Dunnett's test or Student's *t*-test [using STAT VIEW version 5.0 (SAS Institute, Cary, NC)]. $P<0.05$ was considered to indicate statistical significance.

REFERENCES

Brewer, J.W., Hendershot, L.M., Sherr, C.J., Diehl, J.A., 1999. Mammalian unfolded protein response inhibits cyclin D1 translation and cell-cycle progression. Proc. Natl. Acad. Sci. U. S. A. 96, 8505–8510.

Gomer, C., Ferrario, A., Rucker, N., Wong, S., Lee, A.S., 1991. Glucose regulated protein induction and cellular resistance to oxidative stress mediated by porphyrin photosensitization. Cancer Res. 51, 6574–6579.

Hara, H., Onodera, H., Yoshidomi, M., Matsuda, Y., Kogure, K., 1990. Staurosporine, a novel protein kinase C inhibitor, prevents postischemic neuronal damage in the gerbil and rat. J. Cereb. Blood Flow Metab. 10, 646–653.

Helenius, A., 1994. How N-linked oligosaccharides affect glycoprotein folding in the endoplasmic reticulum. Mol. Biol. Cell 5, 253–265.

Ito, D., Tanaka, K., Suzuki, S., Dembo, T., Kosakai, A., Fukuuchi, Y., 2001. Up-regulation of the Ire1-mediated signaling molecule, Bip, in ischemic rat brain. Neuroreport 12, 4023–4028.

Junge, C.E., Sugawara, T., Mannaioni, G., Alagarsamy, S., Conn, P.J., Brat, D.J., Chan, P.H., Traynelis, S.F., 2003. The contribution of protease-activated receptor 1 to neuronal damage caused by transient focal cerebral ischemia. Proc. Natl. Acad. Sci. U. S. A. 100, 13019–13024.

Katayama, T., Imaizumi, K., Sato, N., Miyoshi, K., Kudo, T., Hitomi, J., Morihara, T., Yoneda, T., Gomi, F., Mori, Y., Nakano, Y., Takeda, J., Tsuda, T., Itoyama, Y., Murayama, O., Takashima, A., George-Hyslop, P.S., Takeda, M., Tohyama, M., 1999. Presenilin-1 mutations downregulate the signalling pathway of the unfolded-protein response. Nat. Cell Biol. 1, 479–485.

Katayama, T., Imaizumi, K., Honda, A., Yoneda, T., Kudo, T., Takeda, M., Mori, K., Rozmahel, R., Fraser, P., George-Hyslop, P.S., Tohyama, M., 2001. Disturbed activation of endoplasmic reticulum stress transducers by familial Alzheimer's disease-linked presenilin-1 mutations. J. Biol. Chem. 46, 43446–43454.

Kirino, T., 1982. Delayed neuronal death in the gerbil hippocampus following ischemia. Brain Res. 239, 57–69.

Kirino, T., Sano, K., 1984. Fine structural nature of delayed neuronal death following ischemia in the gerbil hippocampus. Acta Neuropathol. (Berl). 62, 209–218.

Kirino, T., Tamura, A., Sano, K., 1986. A reversible type of neuronal injury following ischemia in the gerbil hippocampus. Stroke 17, 455–459.

Klausner, R.D., Sitia, R., 1990. Protein degradation in the endoplasmic reticulum. Cell. 62, 611–614.

Kudo, T., Kanemoto, S., Hara, H., Morimoto, N., Morihara, T., Kimura, R., Tabira, T., Imaizumi, K., Takeda, M., 2008. A molecular chaperone inducer protects neurons from ER stress. Cell Death Differ. 15, 364–375.

Kuznetsov, G., Chen, L.B., Nigam, S.K., 1997. Multiple molecular chaperones complex with misfolded large oligomeric glycoproteins in the endoplasmic reticulum. J. Biol. Chem. 272, 3057–3063.

Lee, A.S., 1992. Mammalian stress response: induction of the glucose-regulated protein family. Curr. Opin. Cell Biol. 4, 267–273.

Lee, A.S., 2001. The glucose-regulated proteins: stress induction and clinical applications. Trends Biochem Sci. 26, 504–510.

Leroux, L., Desbois, P., Lamote, L., Duvillie, B., Cordonnier, N., Jackerott, M., Jami, J., Bucchini, D., Joshi, R.L., 2001. Compensatory responses in mice carrying a null mutation for Ins1 or Ins2. Diabetes 50, S150–S153.

Loskota, W.J., Lomax, P., Verity, M.A., 1974. A Stereotaxic Atlas of the Mongolian Gerbil Btain (Merones unguiculatus). Ann Arbor Science publishers.

Nishitoh, H., Matsuzawa, A., Tobiume, K., Saegusa, K., Takeda, K., Inoue, K., Hori, S., Kakizaka, A., Ichiijo, H., 2002. ASK1 is essential for endoplasmic reticulum stress-induced neuronal cell death triggered by expanded polyglutamine repeats. Genes Dev. 16, 1345–1355.

Oida, Y., Shimazawa, M., Imaizumi, K., Hara, H., 2008. Involvement of endoplasmic reticulum (ER) stress in the neuronal death induced by transient forebrain ischemia in gerbil. Neuroscience 151, 111–119.

Oyadomari, S., Araki, E., Mori, M., 2002. Endoplasmic reticulum stress-mediated apoptosis in pancreatic beta-cells. Apoptosis 7, 335–345.

Rao, R.V., Peel, A., Logvinova, A., Rio, G., Hermel, E., Yokota, T., Goldsmith, P.C., Ellerby, L.M., Ellerby, H.M., Bredesen, D.E., 2002. Coupling endoplasmic reticulum stress to the cell death program: role of the ER chaperone GRP78. FEBS Lett. 514, 122–128.

Reddy, R.K., Mao, C., Baumeister, P., Austin, R.C., Kaufman, R.J., Lee, A.S., 2003. Endoplasmic reticulum chaperone protein GRP78 protects cells from apoptosis induced by topoisomerase inhibitors: role of ATP binding site in suppression of caspase-7 activation. J. Biol. Chem. 278, 20915–20924.

Roberts, G.G., Di, Loreto, M.J., Marshall, M., Wang, J., Degracia, D.J., 2007. Hippocampal cellular stress responses after global brain ischemia and reperfusion. Antioxid. Redox Signal. 9, 2265–2276.

Ryu, E.J., Harding, H.P., Angelastro, J.M., Vitolo, O.V., Ron, D., Greene, L.A., 2002. Endoplasmic reticulum stress and the unfolded protein response in cellular models of Parkinson's disease. J. Neurosci. 22, 10690–10698.

Shibata, M., Hattori, H., Sasaki, T., Gotoh, J., Hamada, J., Fukuuchi, Y., 2003. Activation of caspase-12 by endoplasmic reticulum stress induced by transient middle cerebral artery occlusion in mice. Neuroscience. 118, 491–499.

Tajiri, S., Oyadomari, S., Yano, S., Morioka, M., Gotoh, T., Hamada, J.I., Ushio, Y., Mori, M., 2004. Ischemia-induced neuronal cell death is mediated by the endoplasmic reticulum stress pathway involving CHOP. Cell Death Differ. 11, 403–415.

Tamatani, M., Matsuyama, T., Yamaguchi, A., Mitsuda, N., Tsukamoto, Y., Taniguchi, M., Che, Y.H., Ozawa, K., Hori, O., Nishimura, H., Yamashita, A., Okabe, M., Yanagi, H., Stern, D.M., Ogawa, S., Tohyama, M., 2001. ORP150 protects against hypoxia/ischemia-induced neuronal death. Nat. Med. 7, 317–323.

Yu, Z., Luo, H., Fu, W., Mattson, M.P., 1999. The endoplasmic reticulum stress-responsive protein GRP78 protects neurons against excitotoxicity and apoptosis: suppression of oxidative stress and stabilization of calcium homeostasis. Exp. Neurol. 155, 302–314.

Anatomical Science International (2008) **83**, 55–59 doi: 10.1111/j.1447-073x.2007.00169.x

Case Report

Nerve fiber analysis on the so-called accessory subscapularis muscle and its morphological significance

Kazuya Yoshinaga[1], Katsushi Kawai[2], Ichiro Tanii[1], Kazunori Imaizumi[1] and Kodo Kodama[2]

1 Department of Anatomy, Faculty of Medicine, University of Miyazaki, Miyazaki, Japan, and
2 Department of Anatomy, Graduate School of Medical Sciences, Kumamoto University, Kumamoto, Japan

Abstract

A rare muscular anomaly, so-called accessory subscapularis muscle, was found in the left axillary fossa of a 95-year-old male cadaver during a student dissection practise. The muscle arose near the lateral margin of the scapula from the surface of the subscapularis muscle and ran upward to fuse with the capsule of the shoulder joint via a tendon. It measured 1.0 cm in width, 7.0 cm in length and 1.5 mm in thickness, and was separated from the underlying subscapularis muscle by the axillary and inferior subscapular nerves. Macroscopically, the anomalous muscle received its nerve supply from a branch arising from the lower root of the radial nerve near the origin of the thoracodorsal nerve and entered the muscle from its ventral surface. Nerve fiber analysis showed that the supplying nerve originated from fibers of the dorsal element of C7 immediately cranial to the thoracodorsal nerve. These findings indicate that the present anomalous muscle might be close to the formation of the latissimus dorsi muscle in its derivation rather than the subscapularis muscle.

Key words: axillary region, brachial plexus, gross anatomy, muscular variation, nerve supply.

Introduction

Muscular variations or accessory muscles in the axillary region of man have often been reported. Clinically, the presence of such anomalous muscles has been pointed out as a possible cause of neurovascular compression in the axilla (Breisch, 1986; Serpell & Baum, 1991; Merida-Velasco *et al.*, 2003). One of the more frequent variations is the axillary arch muscle (achselbogen, axillopectoral muscle or Langer's muscle), which is a transverse muscular band of the axilla extending between the latissimus dorsi and the pectoralis major muscles, occurring in approximately 7–9% of the population (Kasai & Chiba, 1977; Sachatello, 1977; Salmons, 1995). The innervation of the axillary arch muscle has been widely described (Kasai & Chiba, 1977; Sachatello, 1977; Takafuji *et al.*, 1991a; Yuksel *et al.*, 1996; Merida-Velasco *et al.*, 2003).

In contrast, an anomalous muscle occurring on the ventral surface of the subscapularis muscle is a very rare variant and has been referred to as the subscapulo-capsular or subscapulo-humeral muscle (Macalister, 1867), simply the additional slip (Paterson, 1911), the subscapularis minor muscle (Mortensen & Pettersen, 1966), or the accessory subscapularis-teres-latissimus muscle (Kameda, 1976). More recently, it has been termed the accessory subscapularis muscle (Breisch, 1986; Takafuji *et al.*, 1991b). Although observations of these muscles are well documented, their innervations have been indicated only in two publications (Kameda, 1976; Takafuji *et al.*, 1991b), probably because of their deep position in the axillary fossa. It has been reported that such anomalous muscles are innervated by the upper subscapular nerve (Takafuji *et al.*, 1991b), the lower subscapular nerve (Kameda, 1976), a branch of the radial nerve or the thoracodorsal nerve (Kameda, 1976). However, the precise origin of supplying nerves and the derivation of these muscles have not been determined.

During a student dissection course in 2004, we found a case of the anomaly known as the accessory subscapularis muscle. The purpose of the present study was to identify the origin of the nerve supplying this anomalous muscle using a technique for the precise analysis of innervation, and to discuss its derivation and morphological significance.

Materials and methods

When 222 arms from 111 cadavers (61 male, 50 female) were dissected in the gross anatomy course

Correspondence: Kazuya Yoshinaga, Division of Molecular and Cellular Biology, Department of Anatomy, Faculty of Medicine, University of Miyazaki, Kihara 5200, Kiyotake, Miyazaki 889-1692, Japan. Email: kyoshina@med.miyazaki-u.ac.jp
Received 4 April 2006; accepted 4 December 2006.

Figure 1. Ventral view of the left axilla after reflecting the pectoralis major (Pm) and minor (Pmi) muscles to show the anomalous muscle (*), its supplying nerve (arrow) and the brachial plexus. The anomalous muscle compresses the axillary nerve (A) over the subscapularis muscle (Ss). The axillary arch muscle is removed. Ax, axillary artery; Bi, biceps brachii muscle; M, median nerve; R, radial nerve; U, ulnar nerve.

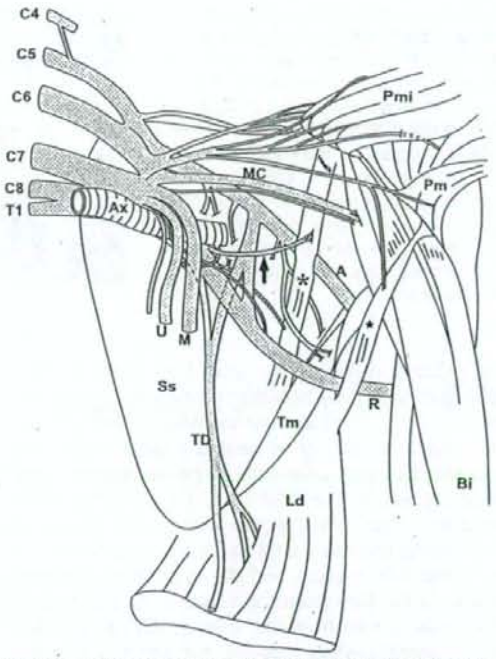

Figure 2. Schematic version of the ventral view of the left axilla, showing the anomalous muscle (*) and its supplying nerve (arrow) in relation to the brachial plexus (shaded) and the surrounding muscles, including the axillary arch muscle (★). A, axillary nerve; Ax, axillary artery; Bi, biceps brachii muscle; Ld, Latissimus dorsi muscle; M, median nerve; MC, musculocutaneous nerve; Pm, pectoralis major muscle; Pmi, pectoralis minor muscle; R, radial nerve; Ss, subscapularis muscle; TD, thoracodorsal nerve; Tm, teres major muscle.

for medical students at University of Miyazaki during a period of 4 years, the present anomalous muscle was found in the cadaver of a 95-year-old Japanese man who had died of heart failure. This anomaly was present in the left axilla, whereas no such anomalous muscle was found in the right axilla. No scars or surgical incisions were observed in the skin of the axilla or upper arm. The structures relative to the anomalous muscle and its innervation were carefully examined. For nerve fiber analysis or fascicular tracing analysis, we detached them from the scapula and humerus together with the brachial plexus. The origin and branching pattern of the nerve supplying the anomalous muscle were examined under a stereomicroscope by stripping off their epineurium with forceps in the water. The findings were recorded as line drawings, measurements and photographs.

The protocol for the present research did not include any specific issue that needed to be approved by the Ethics Committee of University of Miyazaki. The present work conformed to the provisions of the Declaration of Helsinki in 1995 (as revised in Edinburgh 2000; http://www.wma.net/e/policy/b3.htm).

Results

In the left axilla an anomalous muscular slip arose from the surface of the subscapularis muscle at the midpoint of the lateral margin of the scapula, coursed laterally upward and inserted into the shoulder joint capsule along with the tendon of the subscapularis muscle (Figs 1,2). The anomalous muscle was approximately 7.0 cm in length, 1.0 cm in width and 1.5 mm in thickness. It could be distinguished from the underlying subscapularis muscle by the axillary nerve and a caudal branch of the inferior subscapular nerve, which passed between both muscles (Figs 1,2).

As shown in Fig. 2, the formation and branching pattern of the left brachial plexus was unusual, exhibiting type C of Adachi (1928); each anterior division of the upper, middle and lower trunks fused with each other to form a single unit without forming the ansa of the median nerve, and then gave rise to each branch.

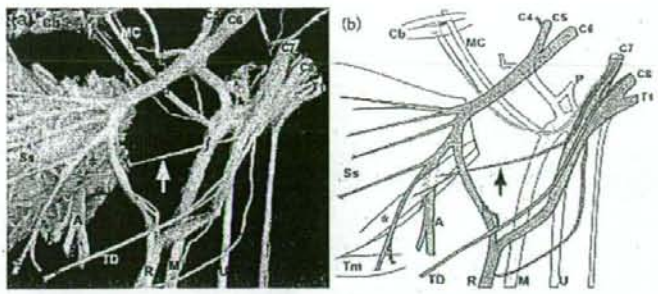

Figure 3. (a) Photograph and (b) schematic version of the dorsal view of nerve fiber analysis of the left brachial plexus, showing that the anomalous muscle (*) is innervated by a branch (arrow) from the dorsal surface of the seventh cervical nerve (C7). The brachial plexus is reflected laterally to show the dorsal parts (shaded) of the plexus. A, axillary nerve; Cb, coracobrachialis muscle; M, median nerve; MC, musculocutaneous nerve; P, pectoral nerve; R, radial nerve; Ss, subscapularis muscle; TD, thoracodorsal nerve; Tm, teres major muscle; U, ulnar nerve.

The posterior division of the upper trunk from the fourth (C4) and sixth (C6) cervical nerves, after giving rise to superior subscapular nerves, was divided into two branches: the axillary nerve and a common branch that split into the upper roots of the radial and thoracodorsal nerves. The inferior subscapular nerve arose near the origin of the axillary nerve, and its cranial and caudal branches entered the lower portion of the subscapularis muscle and the teres major muscle, respectively. The posterior divisions of the middle and lower trunks from the seventh (C7) and eighth (C8) cervical nerves together with the first thoracic nerve (T1) were united to form the lower roots of the radial and thoracodorsal nerves. Both roots of the radial nerve were united at the lower level of the axilla. Thus, the radial and thoracodorsal nerves were formed by the union of the upper and lower roots. Macroscopically, the anomalous muscle appeared to receive its nerve supply from a branch arising from the lower root of the radial nerve near the origin of the thoracodorsal nerve (Fig. 2). The supplying nerve entered the ventral aspect of the anomalous muscle at its midpoint.

To determine the origin of the supplying nerve, nerve fiber analysis was performed under a stereomicroscope (Fig. 3a). After removing the epineurium of the nerves concerned, it was shown that the nerve supplying the anomalous muscle was separated from the other nerve funiculi of C7 and received fibers from the cranial part of the dorsal element of C7 (Fig. 3b). The nerve fiber was located between elements of the thoracodorsal nerve and the deep branch of the musculocutaneous nerve, which supplied the proximal deep part of the coracobrachialis muscle (Koizumi, 1989). The deep branch of the musculocutaneous nerve received fibers from the ventral surface of C7, whereas the thoracodorsal nerve received fibers from the dorsal part of the dorsal elements of C7 (Fig. 3b).

The axillary artery did not penetrate the brachial plexus, but coursed inferior and then posterior to the medial cord of the brachial plexus, compressing the ventral surface of the single posterior division of the middle and lower trunks. The anomalous muscle was supplied by a ramification of the subscapular branch, which arose independently from the proximal region of the axillary artery and passed behind the thoracodorsal and radial nerves (Fig. 2).

In addition to the anomalous muscle, the axillary arch muscle was also present in the left axilla (Fig. 2). It arose from the latissimus dorsi muscle and coursed upwards and laterally towards the axilla to insert into the inferior border of the pectoralis major. The axillary arch muscle crossed ventral to the brachial plexus and the axillary vessels, and was innervated by the most caudal branch of the pectoral nerves, which entered the abdominal part of the pectoralis major muscle (Fig. 2).

Discussion

The present study detailed the gross anatomical findings of an anomalous muscle, which arose from the surface of the subscapularis muscle and passed through the nerves of the posterior cord of the brachial plexus and inserted into the capsule of the shoulder joint. Such anomalous muscular slips with various forms, origins or insertions have been previously described (Macalister, 1867; Paterson, 1911; Mortensen & Pettersen, 1966; Kameda, 1976; Breisch, 1986; Takafuji *et al.*, 1991b). As for the derivation of the anomalous muscle, it was regarded to be a variation of the subscapularis muscle in most of the previous cases, except some cases of Kameda (1976), and was recently termed the accessory subscapularis muscle (Breisch, 1986; Takafuji *et al.*, 1991b). However, judging from the innervation, the present case shows that its possible derivation is not attributable to the subscapularis muscle.

Macroscopically, the present anomalous muscle was innervated by a branch from the lower root of the radial nerve near the origin of the thoracodorsal nerve. This finding and its relation to the plexus were similar to those of cases 5, 6 and 8 of the type II muscle reported by Kameda (1976), although no precise origin of the supplying nerve was determined.

However, the present case was different from those muscles that arose from the latissimus dorsi muscle or from both the subscapularis and latissimus dorsi muscles, and passed between the upper and lower roots of the radial nerve, suggesting the presence of aberrant types of the latissimus dorsi muscle (Kameda, 1976). Concerning the anatomical position and form of the muscle, the present case corresponds to cases 1 and 2 of the type I muscle of Kameda (1976), but these were innervated by the inferior subscapular nerve, suggesting their possible derivation from the teres major muscle. A similar muscular slip was also described by Breisch (1986), who reported a bilateral case of the accessory subscapularis muscle, but did not indicate the innervation.

As a result of nerve fiber analysis of the supplying nerve, we were able to determine the origin of the innervation, and demonstrated that the nerve to the present anomalous muscle was derived from the most cranial fibers of the dorsal element of C7, which was located immediately cranial to the element of the thoracodorsal nerve. It is generally accepted that C7 innervates the subscapularis, teres major and latissimus dorsi muscles and these muscles are embryologically derived from a common muscular origin (Lewis, 1902; Romanes, 1972; Kato, 1989). In the present case, however, C7 innervates the latissimus dorsi muscle and does not innervate the subscapularis and teres major muscles. It would thus seem reasonable to assume that the present anomalous muscle was close to the formation of the latissimus dorsi muscle in its derivation. However, another possibility remains that a part of the teres major muscle, which is innervated by C7, might be isolated to become the anomalous muscle. To our knowledge this is the first report that indicated the origin of the nerve supplying the so-called accessory subscapularis muscle.

Consistent with the findings of the previous cases (Kameda, 1976; Breisch, 1986), the present case passed through the branches of the inferior subscapular nerve. Such a relationship between the muscle and nerves indicates a layer construction of the plexus, and may be the result of the developmental regulatory growth of both structures. It is well known that the nerves of the posterior cord of the brachial plexus are precisely arranged from the dorsocranial to ventrocaudal as follows: the superior subscapular, axillary, inferior subscapular, thoracodorsal and radial nerves (Kato, 1989; Berry *et al.*, 1995). Therefore, it is reasonable that in the present case (i) the second dorsocranial nerve (axillary nerve) passed under the anomalous muscle; (ii) the third dorsocranial nerve (inferior subscapular nerve) passed under and over it; and (iii) the most ventrocaudal nerve (radial nerve) passed over it.

The incidence of the present anomalous muscle reported here is estimated to be 0.45% at University of Miyazaki, although we encountered only one in 222 arms examined. Similar cases were found in at least six of 750 arms (0.8%) in Kumamoto University (K. Kodama, unpubl. data, 2006), 10 of 380 arms (2.6%) by Kameda (1976) and one of 210 arms (0.48%) by Takafuji *et al.* (1991b). Although the incidence of such anomalous muscles is very low and no clinical cases have been reported in the literature, it may be clinically important to be aware of the presence of this variant in the axillary region, because it is possible that the anomalous muscle observed in the present cadaver would compress the axillary and inferior subscapular nerves over the subscapularis muscle and lead to an entrapment neuropathy (Breisch, 1986).

In conclusion, the anomalous muscular slip described here is a very rare variant and its appearance seemed to be an aberrant type of the subscapularis muscle, as reported previously. However, the present findings using nerve fiber analysis show that this anomaly is not associated with the subscapularis muscle, but is closely related to the formation of the latissimus dorsi muscle in its derivation.

Acknowledgment

The authors thank Dr M. Koizumi (Department of Anatomy, Graduate School of Medical Sciences, Kumamoto University) for his helpful comment.

References

Adachi B (1928) *Das Arteriensystem der Japaner*. Bd I. Maruzen, Kyoto.

Berry M, Bannister LH, Standring SM (1995) Nervous system. In: *Gray's Anatomy*, 38th edn (Williams PL, ed.). Churchill Livingstone, New York, 901–1397.

Breisch EA (1986) A rare human variation: The relationship of the axillary and inferior subscapular nerves to an accessory subscapularis muscle. *Anat Rec* **216**, 440–2.

Kameda Y (1976) An anomalous muscle (accessory subscapularis-teres-latissimus muscle) in the axilla penetrating the brachial plexus in man. *Acta Anat* **96**, 513–33.

Kasai T, Chiba S (1977) True nature of the muscular arch of the axilla and its nerve supply. *Acta Anat Nippon* **52**, 309–36 (in Japanese).

Kato K (1989) Innervation of the scapular muscles and its morphological significance in man. *Anat Anz* **168**, 155–68.

Koizumi M (1989) A morphological study on the coracobrachialis muscle. *Acta Anat Nippon* **64**, 18–35 (in Japanese).

Lewis WH (1902) The development of the arm in man. *Am J Anat* **1**, 145–84.

Macalister A (1867) Notes on an instance of irregularity in the muscles around the shoulder joint. *J Anat Physiol* **1**, 316–19.

Merida-Velasco JR, Rodriguez Vazquez JF, Merida Velasco JA, Sobrado Perez J, Jimenez Collado J (2003) Axillary arch: Potential cause of neurovascular compression syndrome. *Clin Anat* **16**, 514–19.

Mortensen OA, Pettersen JC (1966) The musculature. In: *Morris' Human Anatomy*, 12th edn (Anson BJ, ed.). McGraw-Hill, New York, 421–76.

Paterson (1911) The subscapularis muscle. *J Anat Physiol* **46**, 11.

Romanes GJ (1972) *Cunningham's Textbook of Anatomy*, 11th edn. Oxford University Press, London.

Sachatello CR (1977) The axillopectoral muscle (Langer's axillary arch): A cause of axillary vein obstruction. *Surgery* **81**, 610–12.

Salmons S (1995) Muscle. In: *Gray's Anatomy*, 38th edn (Williams PL, ed.). Churchill Livingstone, New York, 737–900.

Serpell JW, Baum M (1991) Significance of 'Langer's axillary arch' in axillary dissection. *Aust NZ J Surg* **61**, 310–12.

Takafuji T, Igarashi J, Kanbayashi T *et al.* (1991a) The muscular arch of the axilla and its nerve supply in Japanese adults. *Acta Anat Nippon* **66**, 511–23 (in Japanese).

Takafuji T, Igarashi J, Kanbayashi T *et al.* (1991b) A very rare and anomalous accessory subscapularis muscle occurring in the axilla of a Japanese adult. *J Med Kyorin Soc* **22**, 397–403 (in Japanese).

Yuksel M, Yuksel E, Surucu S (1996) An axillary arch. *Clin Anat* **9**, 252–4.

Effect of an Inducer of BiP, a Molecular Chaperone, on Endoplasmic Reticulum (ER) Stress-Induced Retinal Cell Death

Yuta Inokuchi,[1] Yoshimi Nakajima,[1] Masamitsu Shimazawa,[1] Takanori Kurita,[2] Mikiko Kubo,[3] Atsushi Saito,[4] Hironao Sajiki,[2] Takashi Kudo,[3] Makoto Aihara,[5] Kazunori Imaizumi,[4] Makoto Araie,[5] and Hideaki Hara[1]

Purpose. The effect of a preferential inducer of 78 kDa glucose-regulated protein (GRP78)/immunoglobulin heavy-chain binding protein (BiP; BiP inducer X, BIX) against tunicamycin-induced cell death in RGC-5 (a rat ganglion cell line), and also against tunicamycin- or *N*-methyl-D-aspartate (NMDA)-induced retinal damage in mice was evaluated.

Methods. In vitro, BiP mRNA was measured after BIX treatment using semi-quantitative RT-PCR or real-time PCR. The effect of BIX on tunicamycin (at 2 μg/mL)-induced damage was evaluated by measuring the cell-death rate and CHOP protein expression. In vivo, BiP protein induction was examined by immunostaining. The retinal cell damage induced by tunicamycin (1 μg) or NMDA (40 nmol) was assessed by examining ganglion cell layer (GCL) cell loss, terminal deoxyribonucleotidyl transferase (TdT)-mediated dUTP nick-end labeling (TUNEL) staining, and CHOP protein expression.

Results. In vitro, BIX preferentially induced BiP mRNA expression both time- and concentration-dependently in RGC-5 cells. BIX (1 and 5 μM) significantly reduced tunicamycin-induced cell death, and BIX (5 μM) significantly reduced tunicamycin-induced CHOP protein expression. In vivo, intravitreal injection of BIX (5 nmol) significantly induced BiP protein expression in the mouse retina. Co-administration of BIX (5 nmol) significantly reduced both the retinal cell death and the CHOP protein expression in GCL induced by intravitreal injection of tunicamycin or NMDA.

Conclusions. These findings suggest that this BiP inducer may have the potential to be a therapeutic agent for endoplasmic reticulum (ER) stress–induced retinal diseases. (*Invest Ophthalmol Vis Sci.* 2009;50:334–344) DOI:10.1167/iovs.08-2123

The endoplasmic reticulum (ER) is the cellular organelle in which proteins (destined for secretion or for diverse subcellular localizations) are not only synthesized, but acquire their correct conformation. Perturbations of the environment normally required for protein folding in the ER, or the production of large amounts of misfolded proteins exceeding the functional capacity of the organelle, trigger a pattern of physiological response in the cell, collectively known as the unfolded protein response (UPR).[1–3] The UPR serves to cope with ER stress by transcriptionally regulating ER chaperones and other ER-resident proteins, attenuating the overall translation rate, and increasing the degradation of misfolded ER proteins. ER stress is caused by the accumulation of unfolded proteins in the ER lumen, and it is associated with various neurodegenerative diseases such as Alzheimer's, Huntington's, and Parkinson's diseases, and with type-1 diabetes.[4–6] Recent reports have shown that ER stress is also involved in a variety of experimental retinal neurodegenerative models, such as those of diabetic retinopathy,[7] retinitis pigmentosa,[8,9] and glaucoma.[10,11]

Recently, we reported that BiP expression is upregulated in the retina after intravitreal injection of either tunicamycin or NMDA (a glutamate-receptor agonist).[12,13] Tunicamycin, a glucosamine-containing nucleoside antibiotic, produced by genus *Streptomyces*, is an inhibitor of *N*-linked glycosylation and the formation of *N*-glycosidic protein-carbohydrate linkages.[14] Tunicamycin, which reduces the *N*-glycosylation of proteins, causes an accumulation of unfolded proteins in the ER and thus induces ER stress. Awai et al.[15] previously had demonstrated that NMDA induces CHOP protein (a member of the CCAAT/enhancer-binding protein family induced by ER stress) in GCL and the inner plexiform layer (IPL), and that CHOP$^{-/-}$ mice are more resistant to NMDA-induced retinal cell death than wild-type mice. These findings indicate that ER stress may be involved in these models of retinal injury.

BiP, a highly conserved member of the 70 kDa heat shock protein family, is one of the chaperones localized to the ER membrane,[16,17] and it is a major ER-luminal Ca^{2+}-storage protein.[18,19] BiP works to restore folding in misfolded or incompletely assembled proteins,[20–22] the interaction between BiP and misfolded proteins being dependent on its hydrophobic motifs.[23–25] Proteins stably bound to BiP are subsequently translocated from the ER into the cytosol, where they are degraded by proteasomes.[26,27] Previous reports have show that induction of BiP prevents the neuronal death induced by ER stress.[28–31] Hence, a selective inducer of BiP might attenuate ER stress and be a new, useful therapeutic agent for the treatment of ER stress-associated diseases.

This seemed an interesting idea, and we recently identified BiP inducer X (BIX) while screening for low molecular

From the Departments of [1]Biofunctional Evaluation, Molecular Pharmacology and [2]Medicinal Chemistry, Gifu Pharmaceutical University, Gifu, Japan; [3]Department of Psychiatry, Osaka University Graduate School of Medicine, Osaka, Japan; [4]Division of Molecular and Cellular Biology, Department of Anatomy, Faculty of Medicine, University of Miyazaki, Miyazaki, Japan; and [5]Department of Ophthalmology, University of Tokyo School of Medicine, Tokyo, Japan.

Supported in part by a Grant-in-Aid (No.18209053) for scientific research from the Ministry of Education, Science, Sports, Culture of the Japanese Government; by a research grant (No.18210101) from the Ministry of Health, Labor, and Welfare of the Japanese Government, and by Grant-in-Aid for Japan Society for the Promotion of Science Fellows.

Submitted for publication April 4, 2008; revised July 25, 2008; accepted October 27, 2008.

Disclosure: **Y. Inokuchi**, None; **Y. Nakajima**, None; **M. Shimazawa**, None; **T. Kurita**, None; **M. Kubo**, None; **A. Saito**, None; **H. Sajiki**, None; **T. Kudo**, None; **M. Aihara**, None; **K. Imaizumi**, None; **M. Araie**, None; **H. Hara**, None

The publication costs of this article were defrayed in part by page charge payment. This article must therefore be marked "*advertisement*" in accordance with 18 U.S.C. §1734 solely to indicate this fact.

Corresponding author: Hideaki Hara, Department of Biofunctional Evaluation, Molecular Pharmacology, Gifu Pharmaceutical University, 5-6-1 Mitahora-higashi, Gifu 502-8585, Japan; hidehara@gifu-pu.ac.jp.

Investigative Ophthalmology & Visual Science, January 2009, Vol. 50, No. 1

mass compounds that might induce BiP using high-throughput screening (HTS) with a BiP reporter assay system (Dual-Luciferase Reporter Assay; Promega Corporation, Madison, WI).[32] We found that BIX preferentially induced BiP mRNA and protein in SK-N-SH cells and reduced tunicamycin-induced cell death. Intracerebroventricular pretreatment with BIX reduced the infarction size after focal cerebral ischemia in mice. In view of the retinal research described above, we wondered whether BIX might reduce the retinal ganglion cell loss and CHOP expression induced by tunicamycin or NMDA treatment.

In the present study, we examined primarily whether induction of BiP might inhibit the retinal cell death induced by tunicamycin in RGC-5 cells in vitro, and/or that induced by tunicamycin or NMDA in mice in vivo.

Materials and Methods

All experiments were performed in accordance with the ARVO Statement for the Use of Animals in Ophthalmic and Vision Research, and they were approved and monitored by the Institutional Animal Care and Use Committee of Gifu Pharmaceutical University, Gifu, Japan.

Materials

Dulbecco modified Eagle medium (DMEM) and NMDA were purchased from Sigma-Aldrich (St. Louis, MO). The other drugs used and their sources were as follows: BIX, 1-(3,4-dihydroxyphenyl)-2-thiocyanatoethanone, was synthesized in the Department of Medicinal Chemistry, Gifu Pharmaceutical University, while tunicamycin was purchased from Wako (Osaka, Japan). Isoflurane was acquired from Nissan Kagaku (Tokyo, Japan) and fetal bovine serum (FBS) was from Valeant (Costa Mesa, CA).

RGC-5 Culture

RGC-5[32] were gifted by Neeraj Agarwal (Department of Pathology and Anatomy, UNT Health Science Center, Fort Worth, TX). Cultures of RGC-5 were maintained in DMEM supplemented with 10% FBS, 100 U/mL penicillin (Meiji Seika Kaisha Ltd., Tokyo, Japan), and 100 μg/mL streptomycin (Meiji Seika Kaisha. Ltd.) in a humidified atmosphere of 95% air and 5% CO_2 at 37°C. The RGC-5 cells were passaged by trypsinization every 3 days, as in our previous reports.[12,13,33] We used RGC-5 without any differentiation.

RNA Isolation and Semi-Quantitative RT-PCR Analysis

To examine the effect of BIX on BiP mRNA expression, RGC-5 cells were seeded in six-well plates at a density of 1.4×10^5 cells per well. After the cells had been incubating for 24 h, they were exposed to 50 μM BIX in 1% FBS DMEM for 0.5, 1, 2, 4, 6, 8, or 12 h, or to 2, 10, 50, or 150 μM BIX in 1% FBS DMEM for 6 h. Total RNA was extracted (RNeasy Mini Kit; QIAGEN KK, Tokyo, Japan) according to the manufacture's protocol. The total RNA was divided into microtubes, and frozen to −80°C. RNA concentrations were determined spectrophotometrically at 260 nm. First-strand cDNA was synthesized in a 20-μl reaction volume using a random primer (Takara, Shiga, Japan) and Moloney murine leukemia virus reverse transcriptase (Invitrogen, Carlsbad, CA). PCR was performed in a total volume of 30 μL containing 0.8 μM of each primer, 0.2 mM dNTPs, 3 U *Taq* DNA polymerase (Promega), 2.5 mM $MgCl_2$, and 1× PCR buffer. The amplification conditions for the semi-quantitative RT-PCR analysis were as follows: an initial denaturation step (95°C for 5 minutes), 20 cycles of 95°C for 1 minute, 55°C for 1 minute, and 72°C for 1 minute, and a final extension step (72°C for 7 minutes). The numbers of amplification cycles for the detection of BiP and β-actin were 18 and 15, respectively. The primers used for amplification were as follows: BiP: 5′-GTTTGCTGAGGAAGACAAAAAGCTC-3′ and 5′-CACTTCCATAGAGTTTGCTGATAATTG-3′; β-actin: 5′-TCCTCCCTGGAGAAGAGCTAC-3′ and 5′-TCCTGCTTGCTGATCCACAT-3′.

PCR products were resolved by electrophoresis through 6% (w/v) polyacrylamide gels. The density of each band was quantified using an imaging program (Scion Image Program; Scion Corporation, Frederick, MD).

Real-Time PCR

Real-time PCR (TaqMan; Applied Biosystems, Foster City, CA) was performed as described previously.[34] Single-stranded cDNA was synthesized from total RNA using a high-capacity cDNA archive kit (Applied Biosystems). Quantitative real-time PCR was performed using a sequence detection system (ABI PRISM 7900HT; Applied Biosystems) with a PCR master mix (TaqMan Universal PCR Master Mix; Applied Biosystems), according to the manufacturer's protocol. mRNA expression was measured by real-time PCR using a gene expression product (Assays-on-Demand Gene Expression Product; Applied Biosystems) and a BiP probe (Assay ID Details: Mm00517691). The thermal cycler conditions were as follows: 2 minutes at 50°C and then 10 minutes at 95°C, followed by two-step PCR for 50 cycles consisting of 95°C for 15 seconds followed by 60°C for 1 minute. For each PCR, we obtained the slope value, R^2 value, and linear range of a standard curve of serial dilutions. All reactions were performed in duplicate. The results are expressed relative to the β-actin (Assay ID Details: Mm00661904) internal control.

Cell Viability

To examine the effects of BIX on the cell death induced by tunicamycin (2 μg/mL) or staurosporine (an ER stress-independent apoptosis inducer, 30 nm) RGC-5 cells were seeded at a low density of 700 cells per well into 96-well plates. After pretreatment with BIX for 12 h, tunicamycin or staurosporine was added to the cultures for 48 h or 24 h, respectively. Cell death was assessed on the basis of combination staining with the fluorescent dyes Hoechst 33342 and propidium iodide (PI; Molecular Probes, Eugene, OR) or the change in fluorescence intensity after the cellular reduction of WST-8 to formazan. Hoechst 33342 (λex 350 nm, λem 461 nm) and PI (λex 535 nm, λem 617 nm) were added to the culture medium at final concentrations of 8 and 1.5 μM, respectively, for 30 minutes. Images were collected using a CCD camera (DP30VW; Olympus America, Center Valley, PA) via an epifluorescence microscope (IX70; Olympus, Tokyo, Japan) fitted with fluorescence filters for Hoechst 33342 (U-MWU; Olympus), and PI (U-MWIG; Olympus). In WST-8 assay, cell viability was assessed by culturing cells in a culture medium containing 10% WST-8 (Cell Counting Kit-8; Dojin Kagaku, Kumamoto, Japan) for 3 h at 37°C, with quantification being achieved by scanning with a microplate reader at 492 nm.[35] This absorbance is expressed as a percentage of that in control cells (which were in 1% FBS DMEM) after subtraction of background absorbance.

Animals

Mice used were male adult ddY mice (Japan SLC, Hamamatsu, Japan), male adult Thy-1-cyan fluorescent protein (CFP) transgenic mice (The Jackson Laboratory, Bar Harbor, Maine),[36] and ER stress–activated indicator (ERAI)-transgenic mice carrying the F-XBP1ΔDBD-venus, a variant of green fluorescent protein (GFP) fusion gene, which allows effective identification of cells under ER stress in vivo, as previously described by Iwawaki et al.[37] Briefly, when ER stress in ERAI transgenic mice was induced, splicing of mRNA encoding the XBP-1 fusion gene occurs and the spliced form of F-XBP1ΔDBD-venus fusion gene could be translated into fluorescent protein. Thus, it is visualized by the fluorescence intensity arising from the XBP-Δ-venus fusion protein during ER stress, and we measured it by fluorescence microscopy and immunoblotting in the present study.

All mice were kept under controlled lighting conditions (12 h:12 h light/dark). The mouse genotype was determined by applying standard PCR methodology to tail DNA.

NMDA- or Tunicamycin-Induced Retinal Damage

NMDA- or tunicamycin-induced retinal damage was produced as previously reported by Siliprandi et al. (1992).[38] Briefly, mice were anesthetized with 3.0% isoflurane and maintained with 1.5% isoflurane in 70% N_2O and 30% O_2 via an animal general anesthesia machine (Soft Lander; Sin-ei Industry Co. Ltd., Saitama, Japan). The body temperature was maintained between 37.0 and 37.5°C with the aid of a heating pad. Retinal damage was induced by the injection (2 μL/eye) of NMDA (Sigma-Aldrich) at 20 mM or tunicamycin at 1 μg/mL dissolved in 0.01 M PBS with 5% dimethyl sulfoxide (DMSO). Each solution was injected into the vitreous body of the left eye under the above anesthesia. One drop of 0.01% levofloxacin ophthalmic solution (Santen Pharmaceuticals Co. Ltd., Osaka, Japan) was applied topically to the treated eye immediately after the intravitreal injection. Seven days after the injection, eyeballs were enucleated for histologic analysis. For comparative purposes, nontreated retinas from each mouse strain were also investigated. BIX (0.5 or 5 nmol) or vehicle (5% DMSO in PBS) was co-administered with the NMDA or tunicamycin in each mouse.

Histologic Analysis

In mice under anesthesia produced by an intraperitoneal injection of sodium pentobarbital (80 mg/kg), each eye was enucleated and kept immersed for at least 24 h at 4°C in a fixative solution containing 4% paraformaldehyde. Six paraffin-embedded sections (thickness, 4 μm) cut through the optic disc of each eye were prepared in a standard manner and stained with hematoxylin and eosin. The damage induced by NMDA or tunicamycin was then evaluated, with three sections from each eye being used for the morphometric analysis, as described below. Light-microscope images were photographed, and the cells in the GCL at a distance between 375 and 625 μm from the optic disc were counted on the photographs in a masked fashion by a single observer (Y.I.). Data from three sections (selected randomly from the six sections) were averaged for each eye and used to evaluate the cell count in the GCL.

Retinal Flatmounts and Analysis in Transgenic Mice

Transgenic mice were given an overdose of sodium pentobarbital, and retinas were dissected out and fixed for 30 minutes in 4% paraformaldehyde diluted in 0.1 M phosphate buffer (PB) at pH 7.4. Retinas were subsequently washed with PBS at room temperature, flatmounted on clean glass slides using fluorescent mounting medium (Dako Corp., Carpinteria, CA), and stored in the dark at 4°C for 1 week. The damage induced by tunicamycin was then evaluated, with four sections (dorsal, ventral, temporal, and nasal) from each eye being used for the morphometric analysis, as described below. At various times after intravitreal injections (24 h in ERAI mice and 7 days in Thy-1-CFP transgenic mice), fluorescent images were photographed (×200, 0.144 mm^2) using an epifluorescence microscope (BX50; Olympus) fitted with a CCD camera (DP30VW; Olympus). In the case of Thy-1-CFP transgenic mice, Thy-1-CFP-positive cells at a distance of 1 mm from the optic disc were counted on the photographs in a masked fashion by a single observer (Y.I.). Data from the four parts of each eye were used to evaluate the RGC count.[39]

Immunostaining

Eyes were enucleated as described under Histologic Analysis, fixed in 4% paraformaldehyde overnight at 4°C, immersed in 25% sucrose for 48 h at 4°C, and embedded in optimum cutting temperature (OCT) compound (Sakura Finetechnical Co. Ltd, Tokyo, Japan). Transverse 10-μm thick cryostat sections were cut and placed onto slides (MAS COAT; Matsunami Glass Ind., Ltd., Osaka, Japan). Immunohistochemical staining was performed according to the following protocol: Briefly, tissue sections were washed in 0.01 M PBS for 10 minutes, and then endogenous peroxidase was quenched by treating the sections with 3% hydrogen peroxide in absolute methanol for 10 minutes, followed by a pre-incubation with 10% normal goat serum. They were then incubated overnight at 4°C with the following primary antibodies: against CHOP (1:1000 dilution in PBS; Santa Cruz, CA), and against BiP/GRP78 (1:1000 dilution in PBS; BD Transduction Laboratories, Lexington, KY). Sections were washed and then incubated with biotinylated anti-rabbit IgG or anti-mouse IgG. They were subsequently incubated with the avidin-biotin-peroxidase complex for 30 minutes, and then developed using diaminobenzidine (DAB) peroxidase substrate. Images were obtained using a digital camera (COOLPIX 4500; Nikon, Tokyo, Japan).

Quantitation of Density

In the DAB-labeled areas of anti-BiP/GRP78 (BD Transduction Laboratories) and anti-CHOP (Santa Cruz) in the GCL and IPL at a distance between 475 and 525 μm (50 × 50 μm) from the optic disc, retinal DAB-labeled cell density was evaluated by means of appropriately calibrated computerized image analysis, using median density in the range of 0 to 255 as an analysis tool (Image Processing and Analysis in Java, Image J; National Institute of Mental Health, Bethesda, MD) and averaged for two areas.[40] The data lie within the dynamic range of this assays

Briefly, light-microscope images of the above-mentioned areas were photographed, inverted in a gradation sequence using image editing software (Adobe Photoshop 5.5; Adobe Systems Inc., San Jose, CA), and then optical intensity was evaluated using Image J. The score for the negative-control (nontreated with first antibody), as the background value, was subtracted from the scores.

TUNEL Staining

TUNEL staining was performed according to the manufacturer's protocol (In Situ Cell Death Detection Kit; Roche Biochemicals, Mannheim, Germany) to detect the retinal cell death induced by NMDA. Mice were anesthetized with pentobarbital sodium at 80 mg/kg, IP, 24 h after intravitreal injection (either of NMDA 40 nmol/eye or of tunicamycin 1 μg/eye). The eyes were enucleated, fixed overnight in 4% paraformaldehyde, and immersed for 2 days in 25% sucrose with PBS. The eyes were then embedded in a supporting medium (OCT compound) for frozen-tissue specimens. Retinal sections at 10-μm thick were cut on a cryostat at −25°C, and stored at −80°C until staining. After twice washing with PBS, sections were incubated with terminal TdT enzyme at 37°C for 1 h, then washed 3 times in PBS for 1 minute at room temperature. Sections were subsequently incubated with an anti-fluorescein antibody-peroxidase conjugate at room temperature in a humidified chamber for 30 minutes, then developed using DAB tetrahydrochloride peroxidase substrate. Light-microscope images were photographed, and the labeled cells in the GCL at a distance between 375 and 625 μm from the optic disc were counted in two areas of the retina in a masked fashion by a single observer (Y.I.). The number of TUNEL-positive cells was averaged for these two areas, and plotted as the number of TUNEL-positive cells.

Western Blot Analysis

RGC-5 cells were lysed using a cell-lysis buffer (RIPA buffer R0278; Sigma-Aldrich) with protease (P8340; Sigma-Aldrich) and phosphatase inhibitor cocktails (P2850 and P5726; Sigma-Aldrich), and 1 mM EDTA. In vivo, mice were euthanatized using sodium pentobarbital at 80 mg/kg, IP, and their eyeballs were quickly removed. The retinas were carefully separated from the eyeballs and quickly frozen in dry ice. For protein extraction, the tissue was homogenized in the cell-lysis buffer using a homogenizer (Physcotron; Microtec Co. Ltd., Chiba, Japan). The lysate was centrifuged at 12,000*g* for 20 minutes, and the supernatant was used for this study. Assays to determine the protein concentration were performed by comparison with a known concentration of bovine serum albumin using a BCA protein assay kit (Pierce Biotechnology, Rockford, IL). A mixture of equal parts of an aliquot of

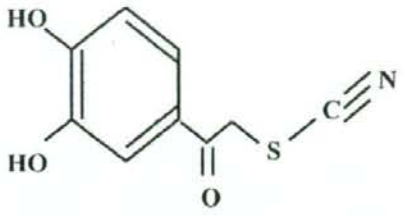

FIGURE 1. The structure of BIX (1-(3,4-dihydroxyphenyl)-2-thiocyanate-ethanone).

protein and sample buffer with 10% 2-mercaptoethanol was subjected to 10% sodium dodecyl sulfate-polyacrylamide gel electrophoresis. The separated protein was then transferred onto a polyvinylidene difluoride membrane (Immobilon-P; Millipore Corporation, Bedford, MA). For immunoblotting, the following primary antibodies were used: rabbit anti-CHOP polyclonal antibody (1:1000; Santa Cruz), mouse anti-β-actin monoclonal antibody (1:4000; Sigma-Aldrich), and rabbit anti-green fluorescent protein (GFP) polyclonal antibody (1:1000; Medical & Biological Laboratories Co. Ltd., Nagoya, Japan). The secondary antibody used was either goat anti-rabbit HRP-conjugated (1:2000) or goat anti-mouse HRP-conjugated (1:2000). The immunoreactive bands were visualized using a chemiluminescent substrate (SuperSignal West Femto Maximum Sensitivity Substrate; Pierce Biotechnology). The band intensity was measured using an imaging analyzer (Lumino Imaging Analyzer; Toyobo, Osaka, Japan) and a gel analysis electrophoresis analysis software (Gel Pro Analyzer; Media Cybernetics, Atlanta, GA).

Statistical Analysis

Data are presented as the means ± SE. Statistical comparisons were made by way of Dunnett's test or Student's *t*-test using statistical analysis software (STAT VIEW version 5.0; SAS Institute, Cary, NC). $P < 0.05$ was considered to indicate statistical significance.

RESULTS

BiP mRNA in RGC-5 Preferentially Induced by BIX

To clarify whether BIX (Fig. 1) induces BiP in RGC-5, we used semi-quantitative RT-PCR and real-time PCR, using a specific primer and a TaqMan probe recognizing BiP mRNA, respectively. Real-time PCR revealed that the level of BiP mRNA was significantly elevated at 0.5 to 12 h (peak at approximately 6 h) after treatment with 50 μM BIX (Fig. 2A). At 6 h after treatment with BIX (2 to 150 μM), BiP mRNA was increased concentration-dependently (Fig. 2B). Next, we used real-time *PCR* to investigate whether BIX might affect the expressions of any other genes related to the ER stress response, such as GRP94, calreticulin, protein kinase inhibitor of 58 kDa ($p58^{IPK}$), or asparagine synthetase (ASNS; Fig. 2C). Real-time PCR revealed significant inductions of ASNS and calreticulin mRNAs at 6 h after treatment with BIX at 2 and 10 μM, respectively. At 50 μM, BIX induced the mRNAs for GRP94 at 12 h, calreticulin at 6 and 12 h, $p58^{IPK}$ at 6 h, and ASNS at 12 h. In contrast, GRP94 mRNA was significantly reduced at 4 h after treatment with 50 μM BIX.

Protective Effect of BIX against ER Stress–Induced Cell Death in RGC-5 Cells

To investigate whether BIX can prevent the cell death induced by ER stress, RGC-5 cells were pretreated for 12 h with or without BIX, then treated with 2 μg/mL tunicamycin, and finally incubated for a further 48 h. Fluorescence micrographs of Hoechst 33342 and PI staining revealed 38.4 ± 4.5% cell death ($n = 8$) at 48 h after tunicamycin treatment, (control: 0.9 ± 0.2%, $n = 8$), and pretreatment with BIX at 1 and 5 μM significantly reduced this cell death (Figs. 3A, 3B). Next, we evaluated the expression of CHOP protein after tunicamycin treatment. There was no CHOP protein expression in either nontreated or BIX-treated cells (Figs. 3C, 3D). On the other

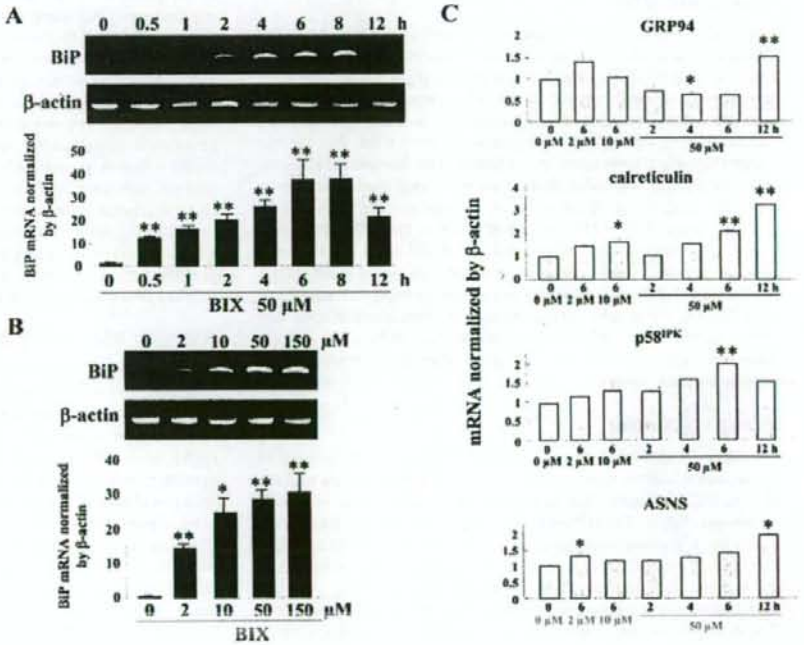

FIGURE 2. Effect of BIX on BiP mRNA expression BIX in RGC-5 cells. (**A**) Time-dependent induction of BiP mRNA after treatment with 50 μM BIX and (**B**) concentration-dependence of BIX-induced BiP mRNA expression are each shown by semi-quantitative RT-PCR (*upper panel*) and real-time PCR (*lower panel*). β-Actin mRNA is shown as an internal control. (**C**) Induction of GRP94, calreticulin, $p58^{IPK}$, and ASNS mRNAs at 6 h after treatment with 2 or 10 μM BIX and at 2 to 12 h after treatment with 50 μM BIX. Data are shown as mean ± SE ($n = 3$ or 4). $^{*}P < 0.05$, $^{**}P < 0.01$ versus 0 μM (A and B) or 0 μM/0 h (C).

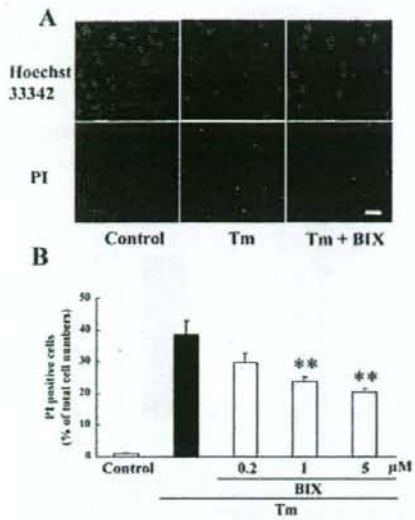

FIGURE 3. Effects of BIX on tunicamycin-induced cell death and CHOP protein expression in RGC-5 cells. (A) RGC-5 cells were pretreated with vehicle or with 1 μM BIX for 12 h, and then immersed in fresh medium (control) or in medium supplemented with 2 μg/mL tunicamycin (Tm; labeled Tm or Tm + BIX). *Upper* photomicrographs show Hoechst 33342 and *lower* ones propidium iodide (PI) staining at 48 h after tunicamycin stimulation. Scale bar represents 25 μm. (B) Numbers of PI-positive cells after tunicamycin treatment. Pretreatment of cells with BIX (1 and 5 μM) significantly reduced the amount of cell death (vs. cells treated with tunicamycin alone). (C) Immunoblot of CHOP protein shows that tunicamycin induced significant CHOP expression, and that pretreatment of cells with BIX at 5 μM reduced this expression with no change in the level of β-actin. *Upper panel* shows CHOP and *lower panel* shows β-actin. (D) Quantitative representations of β-actin-based tunicamycin-induced CHOP protein expression (in arbitrary units). Data are shown as mean ± SE ($n = 6$ or 8). $^*P < 0.05$, $^{**}P < 0.01$ versus tunicamycin alone.

hand, tunicamycin markedly induced CHOP protein, while pretreatment with BIX at 5 μM reduced this expression to almost half the value seen after tunicamycin treatment alone (Figs. 3C, 3D).

Effects of BIX on Cell Damage Induced by Staurosporine in RGC-5 Culture

To investigate whether BIX protects non-ER stress-induced cell death, we examined staurosporine-induced cell death. Staurosporine at 30 nM for 24 h reduced cell viability to approximately 60% of control (Fig. 4). There was no statistical difference between BIX (1 and 5 μM)-treated and vehicle-treated group.

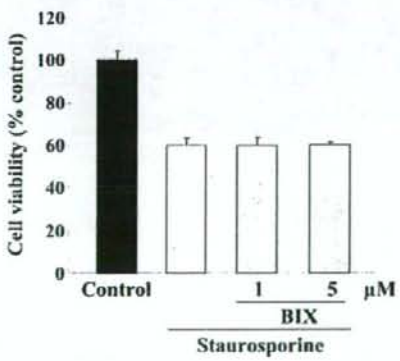

FIGURE 4. Effect of BIX on the cell death induced by staurosporine in RGC-5. RGC-5 cells were pretreated with vehicle or with BIX (1 or 5 μM) for 12 h, and then immersed in fresh medium (control) or in medium supplemented with staurosporine at 30 nM. At the end of this culture period, cell death was assessed by WST-8 assay (Cell Counting Kit-8; Dojin Kagaku). Data are shown as mean ± SE ($n = 6$).

BiP Protein in the Mouse Retina Induced by Intravitreous Injection of BIX

Compared with that in the nontreated retina, BiP protein expression in GCL and IPL was significantly increased at 6 and 12 h after intravitreal injection of BIX (5 nmol; Figs. 5A, 5B). Optical density analysis confirmed that administration of BIX induced BiP protein in vivo (Fig. 5D).

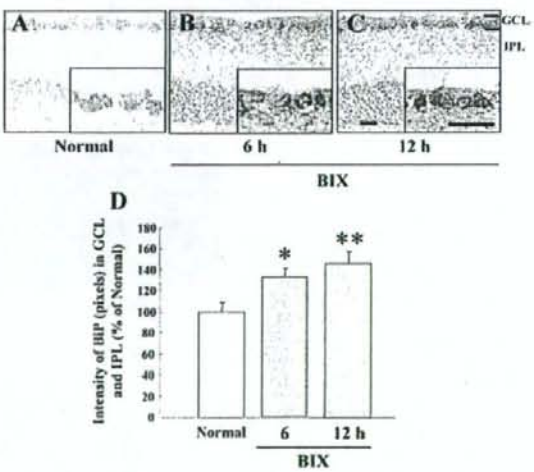

FIGURE 5. BiP protein expression in the mouse retina induced by intravitreous injection of BIX. Immunostaining probed with an antibody against BiP/GRP78. (A) Nontreated, (B) 6 h, and (C) 12 h after intravitreous injection of BIX (5 nmol). (D) Expression ratio for BiP induction intravitreous injection of BIX is represented as the ratio of intensity values. Data are shown as mean ± SE ($n = 6$). $^*P < 0.05$, $^{**}P < 0.01$ versus nontreated normal retina. Each scale bar represents 25 μm.

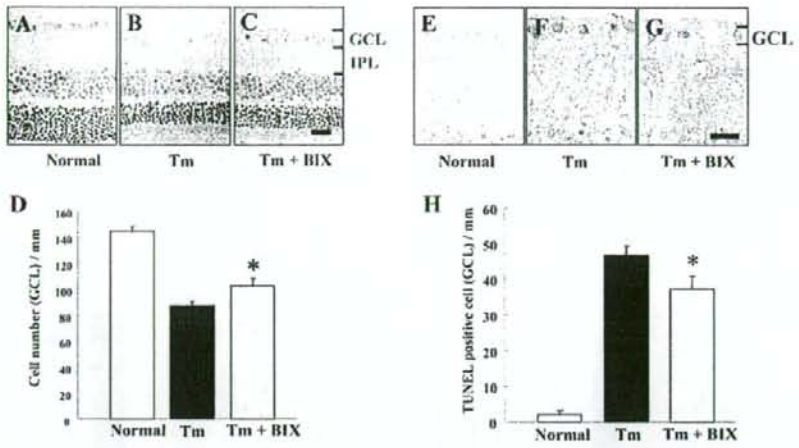

FIGURE 6. Effects of BIX on retinal damage induced by intravitreal injection of tunicamycin in mice. Hematoxylin and eosin staining of cross-sections of (A) nontreated, (B) Tm-treated, and (C) Tm plus BIX-treated mouse retinas at seven days after intravitreal injection of tunicamycin (1 μg) either alone or with BIX (5 nmol). (D) Damage was evaluated by counting cell numbers in GCL at seven days after the above injections. TUNEL staining of cross-sections of (E) nontreated, (F) Tm-treated, and (G) Tm plus BIX-treated mouse retinas at seven days after the above injections. (H) Effect of BIX on Tm-induced expression of TUNEL-positive cells at 24 h after the above injections. Data are shown as mean ± SE ($n = 9$ or 10). *$P < 0.05$ versus tunicamycin alone. Scale bars each represent 25 μm.

Protective Effect of BIX against Tunicamycin-Induced Retinal Damage in Mice

Tunicamycin decreased the cell number in GCL at 7 days after its intravitreal injection (vs. nontreated retinas; Figs. 6A, 6B). There was significantly less cell loss in GCL when BIX (5 nmol) was co-administered with the tunicamycin (Figs. 6B–6D). In addition, intravitreal injection of tunicamycin increased the number of TUNEL-positive cells in GCL at 24 h (vs. nontreated retinas; Figs. 6E, 6F). BIX (5 nmol), when co-administered with the tunicamycin, significantly reduced the number of TUNEL-positive cells (vs. tunicamycin alone; Figs. 6F–6H).

Protective Effect of BIX against Tunicamycin-Induced Retinal Damage in Thy-1-CFP Transgenic Mice

In this experiment on Thy-1-CFP transgenic mice, we confirmed the effect of BIX in a larger retinal area than that evaluated in Figure 6D. We counted the number of Thy-1-CFP-positive cells (in flatmounts) in the four white areas shown 1 mm from the center of the optic disc in Figure 7E, and then totaled these values. In the Thy-1-CFP–transgenic mouse retina, axonal fibers were evenly and densely distributed. There were congested CFP-positive cells in the vehicle-treated retina (Fig. 7A), and no change was observed in BIX-treated retinas without tunicamycin treatment (Fig. 7B). Intravitreal injection of tunicamycin decreased the Thy-1-CFP–positive cell count at 7 days (vs. vehicle-treated retina; Figs. 7A, 7C). BIX at 5 nmol, when co-administered with the tunicamycin, significantly inhibited this cell loss (Figs. 7C, 7D, 7F).

Effect of BIX on Tunicamycin-Induced CHOP Expression in Mice

Representative photograph of a nontreated retina is shown in Figure 8A. No change was observed in the BIX-treated retina (Fig. 8B). Optical density analysis of CHOP protein immunoreactivity in GCL and IPL showed that intravitreal injection of tunicamycin (1 μg) significantly increased the level of CHOP protein at 72 h after the injection (Fig. 8C). BIX (5 nmol), when co-administered with the tunicamycin, significantly inhibited this effect (Figs. 8D, 8E).

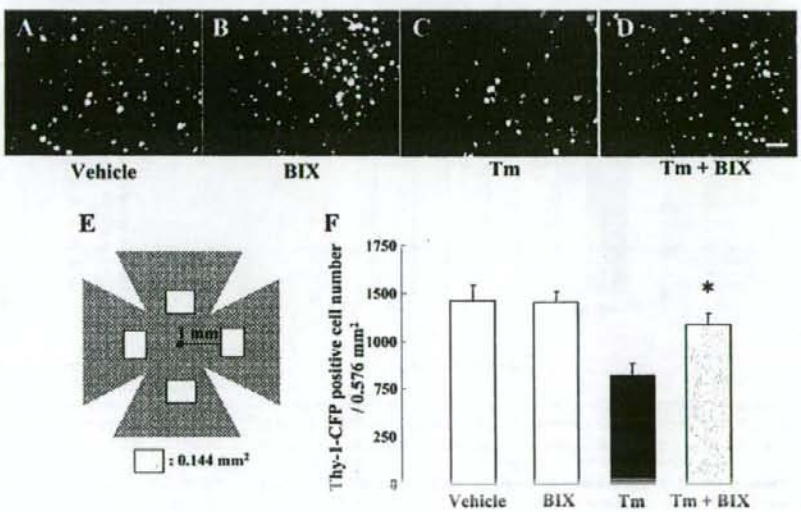

FIGURE 7. Effects of BIX on retinal damage induced by intravitreal injection of tunicamycin in Thy-1-CFP transgenic mice. Mouse retinas (flatmounts) at seven days after intravitreal injection of (A) vehicle, (B) BIX (5 nmol), (C) Tm (1 μg), or (D) Tm (1 μg) plus BIX (5 nmol). Damage was evaluated by counting Thy-1-CFP–positive cell numbers in the four *white* areas shown in (E) (each area 0.144 mm² × 4 areas; total 0.576 mm²) at seven days after the above intravitreal injections. (F) Effect of BIX against Tm-induced damage (indicated by decreased number of Thy-1-CFP–positive cells) at seven days after intravitreal injection. Data are shown as mean ± SE ($n = 9$ or 10). *$P < 0.05$ versus tunicamycin alone. Scale bar represents 25 μm.

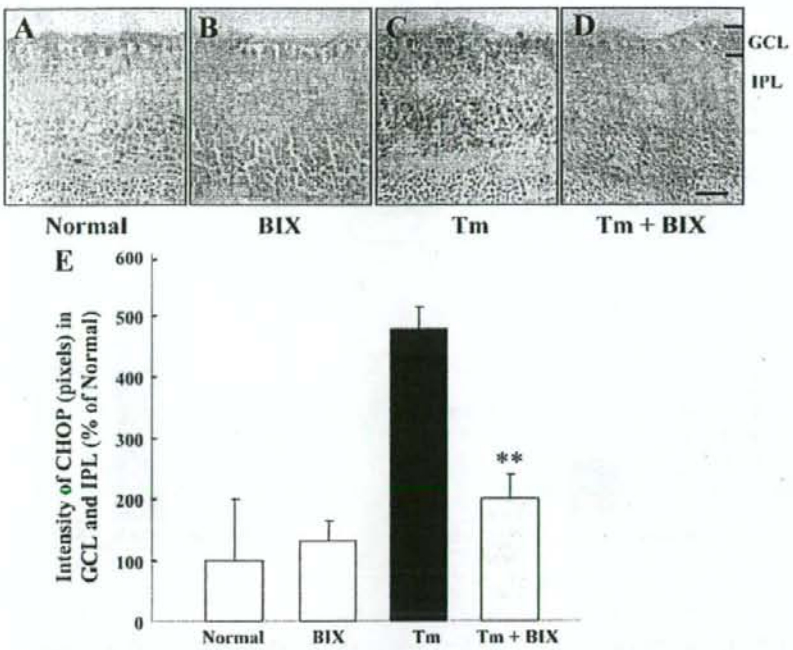

FIGURE 8. Effect of BIX on tunicamycin-induced CHOP expression in the mouse retina. Mouse retinas (cross-sections) either (A) nontreated or at three days after intravitreal injection of (B) BIX (5 nmol), (C) Tm (1 μg) or (D) Tm (1 μg) plus BIX (5 nmol). (E) Relative density of CHOP protein expression in GCL and IPL at three days after the above intravitreal injections. Data are shown as mean ± SE ($n = 6$). $^{**}P < 0.01$ versus tunicamycin alone. Scale bar represents 25 μm.

Effect of BIX on Tunicamycin-Induced XBP-1 Expression in ERAI Mice

In ERAI mice, the fluorescence intensity arising from the XBP-1–venus fusion protein (indicating ER stress activation) can be easily visualized, allowing evaluation of the effect of ER stress on the retina. In the representative photographs of flatmount retinas from ERAI mice shown in Figure 9, no difference was observed between vehicle-treated and BIX-treated retinas (Fig. 9B). Intravitreal injection of tunicamycin (1 μg) induced XBP-1–venus expression (vs. the vehicle-treated retina; Fig. 9C). Immunoblot analysis of XBP-1–venus protein expression in the retina (using an anti-GFP antibody) showed that intravitreal injection of tunicamycin (1 μg) significantly raised the level of XBP-1–venus protein, and that BIX (5 nmol), when co-administered with the tunicamycin (Fig. 9D), significantly inhibited this effect (Figs. 9E, 9F).

Protective Effect of BIX against NMDA-Induced Retinal Damage in Mice

A representative photograph of a nontreated retina is shown in Figure 10A. Intravitreal injection of NMDA (a) decreased the

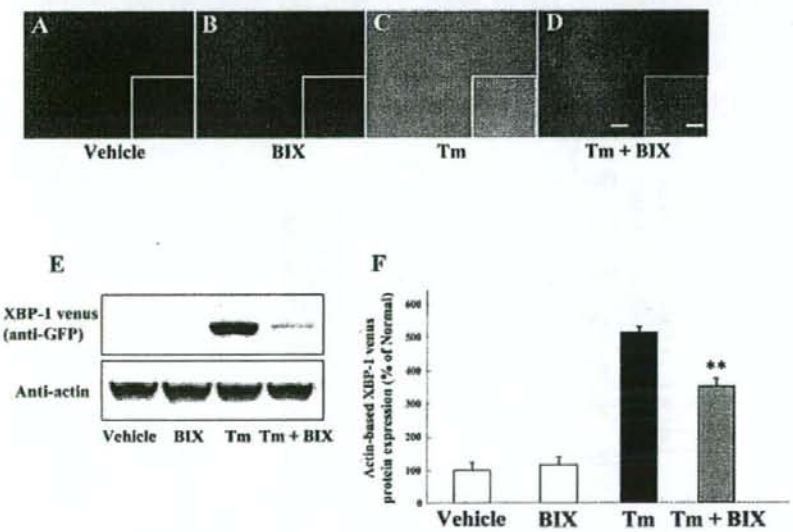

FIGURE 9. Effect of BIX on tunicamycin-induced XBP-1 venus expression in ERAI mice. Mouse retinas (flatmounts) at 24 h after intravitreal injection of (A) vehicle, (B) BIX (5 nmol), (C) Tm (1 μg) or (D) Tm (1 μg) plus BIX (5 nmol). (E) *Upper panel* shows XBP-1 venus protein expression, while *lower panel* shows β-actin protein expression at 24 h after the above injections. (F) Western blot analysis showing effect of BIX on Tm-induced expression of β-actin-based XBP-1 venus protein expression at 24 h after the above injections. Data are shown as mean ± SE ($n = 8$). $^{*}P < 0.01$ versus tunicamycin alone. Scale bars in main photomicrographs and in *insets* represent 25 and 5 μm, respectively.

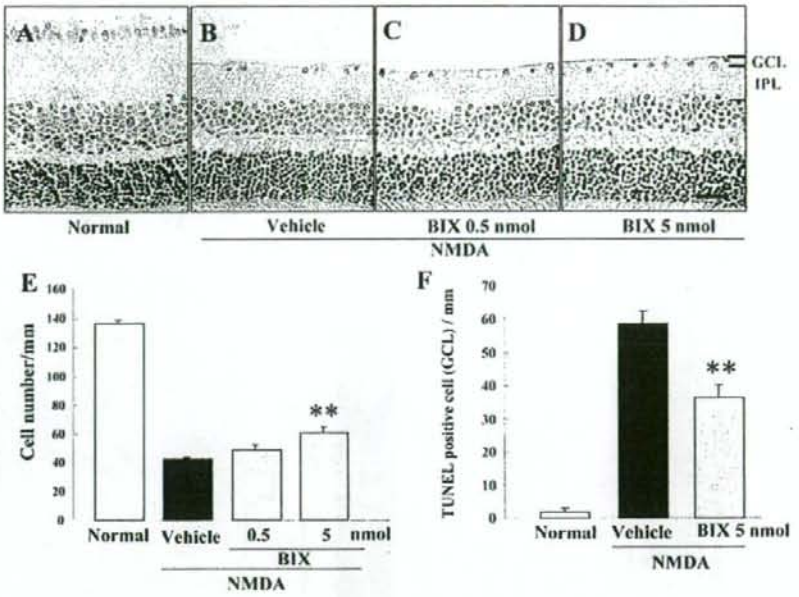

FIGURE 10. Effects of BIX on retinal damage induced by intravitreal injection of NMDA in mice. Mouse retinas (cross-sections) either (A) nontreated or at seven days after intravitreal injection of (B) NMDA (40 nmol) alone or (C, D) NMDA (40 nmol) plus BIX (0.5 or 5 nmol). (E) Damage was evaluated by counting cell numbers in GCL at seven days after the above intravitreal injections. (F) Effect of BIX on NMDA-induced expression of TUNEL-positive cells at 24 h after intravitreal injection of NMDA (40 nmol) either alone or with BIX (5 nmol). Data are shown as mean ± SE ($n = 9$ or 10). $^{**}P < 0.01$ versus NMDA-treated control group. Scale bar represents 25 μm.

cell number in GCL at 7 days (Figs. 10B, 10E) and (b) increased the number of TUNEL-positive cells in GCL at 24 h (vs. nontreated normal retina; Fig. 10F). BIX (5 nmol), when co-administered with the NMDA, significantly reduced (vs. NMDA alone) both the cell loss in GCL (Figs. 10D, 10E) and the number of TUNEL-positive cells (Fig. 10F). On the other hand, there was no statistical difference between BIX (0.5 nmol)- and vehicle-treated group in NMDA-induced cell death in GCL (Figs. 10C, 10E).

Effect of BIX on NMDA-Induced CHOP Expression in Mice

A representative photograph of a nontreated retina is shown in Figure 11A and no change was detected between nontreated

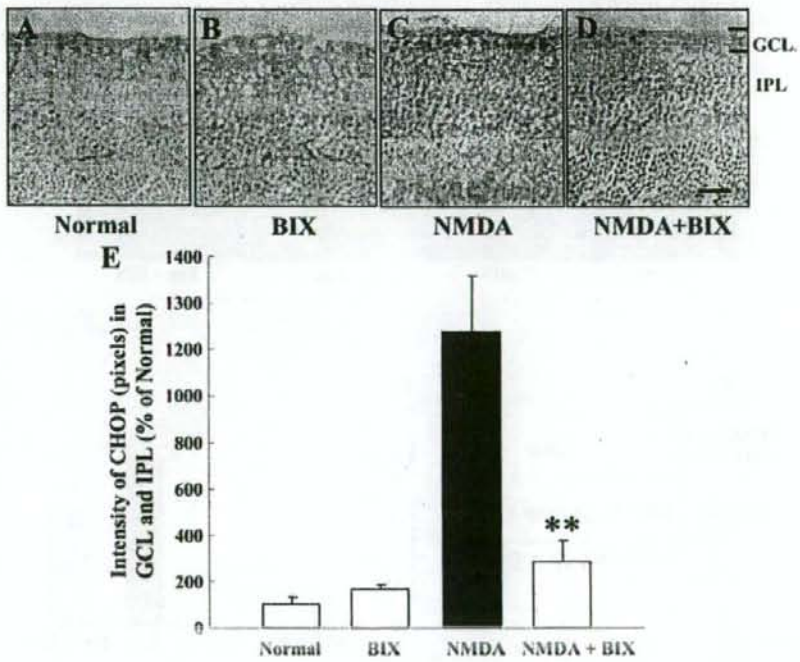

FIGURE 11. Effect of BIX on NMDA-induced CHOP expression in mice. Mouse retinas (cross-sections) either (A) nontreated or at three days after intravitreal injection of (B) NMDA (40 nmol) alone or (C) NMDA (40 nmol), or (D) NMDA (40 nmol) plus BIX (5 nmol). (E) Relative density of CHOP protein expression in GCL and IPL at three days after the above intravitreal injections. Data are shown as mean ± SE ($n = 6$). $^{**}P < 0.01$ versus NMDA alone. Scale bar represents 25 μm.

retina and the BIX-treated retina without NMDA treatment (Figs. 11A, 11B). Optical density analysis of CHOP protein immunoreactivity in GCL and IPL showed that intravitreal injection of NMDA (40 nmol) significantly increased the level of CHOP protein at 72 h after the injection (Fig. 11C). When co-administered with the NMDA, BIX (5 nmol) significantly inhibited this effect (Figs. 11D, 11E).

Discussion

In the present study, we confirmed that BIX preferentially induces BiP mRNA in RGC-5. Although it also induced GRP94, calreticulin, $p58^{IPK}$, and ASNS, these inductions were lower than that of BiP. This is consistent with our previous study that BIX preferentially induced BiP with slight inductions of GRP94, calreticulin, and CHOP mediated by the activating transcription factor 6 (ATF6) pathway accompanied by activation of ERSEs, and that BIX does not affect the pathway downstream of IRE1 or the translational control branch downstream of PERK in SK-N-SH cells.[32] Therefore, BIX is not just an ER stressor such as tunicamycin or thapsigargin, and we consider that the induction of BiP by BIX is mediated by the ATF6 pathway in RGC-5 similar to that in SK-N-SH cells. Next, we evaluated the effects of BIX, as a preferential inducer of BiP, on ER stress-induced in vitro cell death in RGC-5 (a rat ganglion cell-line) and in vivo retinal damage in mice. We found that BIX reduced tunicamycin-induced cell death in RGC-5 and also reduced both tunicamycin-induced and NMDA-induced retinal damage in mice. Our previous study revealed that BIX (a) reduced tunicamycin-induced cell death in SK-N-SH cells, (b) contributed to the induction of BiP expression via the ATF-6 pathway (but not via the PERK or IRE1 pathways), and (c) on intracerebroventricular injection, prevented the neuronal damage induced by focal ischemia in mice.[32] Furthermore, immunostaining revealed that intravitreal injection of BIX significantly induced BiP protein in mouse retina. Particularly, it expressed in GCL and IPL (versus both the normal and the sham retina). On the other hand, there was little protective effect of BIX against RGC-5 damages after staurosporine treatment. Staurosporine is well known as a nonspecific inhibitor of protein kinases and initiates caspase-dependent apoptosis in many cell types.[41,42] Our previous studies revealed that staurosporine induced cell death without any changes in the expression of BiP or CHOP protein.[12,43] Furthermore, preliminary study showed that treatment with BIX (1 and 5 μM) did not inhibit RGC-5 cell death 48 h after serum deprivation, which does not induce any UPR-responses such as BiP or CHOP (unpublished data). These results strongly support that BIX selectively protects cell damage induced by ER stress.

Recently, we reported that in mice, increased expressions of XBP-1 splicing, BiP, and CHOP could be detected after the induction of retinal damage by tunicamycin, NMDA, or an elevation of intraocular pressure.[13] That report was the first to demonstrate an involvement of ER stress and BiP in retinal cell death in mice. Hence, in the present study we asked whether BIX can prevent such retinal damage. By histologic analysis and TUNEL staining, we estimated that BIX reduced tunicamycin-induced retinal damage in GCL. However, the cell counts in partial cross sections provide a comparatively small sample on which quantitative morphometry can be used to judge such an effect. Therefore, we used Thy-1-CFP transgenic mice[36] to examine the effect of BIX in a large retinal area. This transgene contains a CFP gene under the direction of regulatory elements derived from the mouse Thy-1 gene, and the transgenic mice express CFP protein in RGC and in the inner part of the IPL of the retina.[36] Our results show that BIX exerted a protective effect against tunicamycin-induced retinal damage in the Thy-1-CFP transgenic mouse. However, it is possible that microglial cells become co-labeled with CFP by phagocytosis of the dying RGCs. In this study, we evaluated CFP-positive cells in 7 days after tunicamycin injection. In our previous and preliminary studies, activated microglia cells in GCL were increased at 3 days after NMDA injection[13] and their increases were almost ceased within the 7 days (unpublished data). Furthermore, microglial cells can be distinguished with neuronal cells by their morphologic features.[44] In fact, microglial cells were scarcely observed at seven days after tunicamycin injection, similar to that at seven days after NMDA injection. When we investigated the effect of BIX on NMDA-induced retinal damage in ddY mice, we found that it significantly attenuated such damage. NMDA is well known to induce RGC death and optic-nerve loss (effects mediated by excitatory glutamate receptor), and such neuronal death is believed to play a role in many neurologic and neurodegenerative diseases.[45,46] Recently, Uehara et al.[47] noted that mild exposure to NMDA induced apoptotic cell death in primary cortical culture, and they demonstrated this effect to be caused by an accumulation of polyubiquitinated proteins and increases in XBP-1 mRNA splicing and CHOP mRNA (reflecting activation of the UPR signaling pathway). They also found that protein-disulphide isomerase, which assists in the maturation and transport of unfolded secretory proteins, prevented the neurotoxicity associated with ER stress. These findings suggested that activation of ER stress may participate in the retinal cell death occurring after NMDA-receptor activation and/or an ischemic insult.[47]

In our investigation of the mechanisms underlying the above-mentioned effects, we focused on CHOP. Since CHOP is a member of the CCAAT/enhancer-binding protein family that is induced by ER stress and participates in ER-mediated apoptosis, CHOP may be a key molecule in retinal cell death.[48] We found that treatment with tunicamycin induced apoptotic cell death in RGC-5 and also induced a production of ER stress-related proteins (BiP, the phosphorylated form of eIF2α, and CHOP protein). BIX reduced both the cell death and the CHOP protein expression induced by tunicamycin in RGC-5 in vitro. BIX also attenuated the CHOP protein expression induced by either tunicamycin or NMDA in the mouse retina in vivo. As mentioned above, BIX may affect CHOP protein expression through ATF6 pathway, but no change was observed in BIX-treated RGC-5. In our previous data in SK-N-SH cells, BIX slightly increased CHOP mRNA only at 2 h after the treatment. Expression of CHOP is mainly regulated by three transcription factors—ATF4, cleaved ATF6, and x-box binding protein-1 (XBP-1)—which are downstream effectors during ER stress in similar to other ER chaperones. These differences between BiP and CHOP expression by BIX may be due to the difference of their promoters. CHOP promoter contains at least two ERSE motifs (CHOP ERSE-1 and CHOP ERSE-2) located in opposite directions with a 9 bp overlap, and one of ERSEs is inactive.[49] On the other hand, BiP promoter has three functional ERSE motifs of the rat GRP78 promoter (ERSE-163, ERSE-131, and ERSE-98).[50] These variations in each promoter may contribute to the differences among the expressions of ER chaperons induced by BIX and the lack of CHOP expression.

Subsequently, we monitored XBP-1 activation in the mouse retina in vivo, using ERAI transgenic mice.[37] Effective identification of cells under ER stress conditions is possible in the retina in these mice, as described in our previous report.[13] Here, ERAI mice carrying the F-XBP1ΔDBD-venus expression gene were used to monitor ER stress. The fluorescence intensity arising from the X-box binding protein (XBP1)-venus fusion protein, indicating ER stress activation, was increased in cells within GCL and IPL at 24 h after injection of tunicamycin into the vitreous. BIX significantly reduced this expression, indicating that BIX may attenuate the retinal damage induced

by ER stress-associated factors. In our previous study,[32] we found that BIX induced BiP protein expression via the ATF-6 pathway (not via other ER stress-associated factors such as the PERK and IRE1 pathways) in SK-N-SH cells. Possibly, the protective mechanism underlying the effect of BIX on the mouse retina may be the same as that revealed by our previous study, but further experiments will be needed to clarify this issue.

In conclusion, we have demonstrated that BIX, a preferential inducer of BiP, inhibits both the neuronal cell death induced by ER stress in vitro in RGC-5 cells and in vivo in the mouse retina. Hence, an increase in BiP might be one of the targets of mechanisms bestowing neuroprotection in retinal diseases.

Acknowledgments

The authors thank Masayuki Miura (Department of Genetics, Graduate School of Pharmaceutical Sciences, University of Tokyo, Tokyo, Japan) for the kind gift of ERAI mice, and Rumi Uchibayashi and Shunsake Imai for technical assistance.

References

1. Travers KJ, Patil CK, Wodicka L, Lockhart DJ, Weissman JS, Walter P. Functional and genomic analyses reveal an essential coordination between the unfolded protein response and ER-associated degradation. *Cell.* 2000;101:249–258.
2. Harding HP, Novoa I, Zhang Y, et al. Regulated translation initiation controls stress-induced gene expression in mammalian cells. *Mol Cell.* 2000;6:1099–1108.
3. Schroder M, Kaufman RJ. The mammalian unfolded protein response. *Annu Rev Biochem.* 2005;74:739–789.
4. Katayama T, Imaizumi K, Honda A, et al. Disturbed activation of endoplasmic reticulum stress transducers by familial Alzheimer's disease-linked presenilin-1 mutations. *J Biol Chem.* 2001;276:43446–43454.
5. Ryu EJ, Harding HP, Angelastro JM, Vitolo OV, Ron D, Greene LA. Endoplasmic reticulum stress and the unfolded protein response in cellular models of Parkinson's disease. *J Neurosci.* 2002;22:10690–10698.
6. Oyadomari S, Koizumi A, Takeda K, et al. Targeted disruption of the Chop gene delays endoplasmic reticulum stress-mediated diabetes. *J Clin Invest.* 2002;109:525–532.
7. Roybal CN, Yang S, Sun CW, et al. Homocysteine increases the expression of vascular endothelial growth factor by a mechanism involving endoplasmic reticulum stress and transcription factor ATF4. *J Biol Chem.* 2004;279:14844–14852.
8. Rebello G, Ramesar R, Vorster A, et al. Apoptosis-inducing signal sequence mutation in carbonic anhydrase IV identified in patients with the RP17 form of retinitis pigmentosa. *Proc Natl Acad Sci USA.* 2004;101:6617–6622.
9. Lin JH, Li H, Yasumura D, et al. IRE1 signaling affects cell fate during the unfolded protein response. *Science.* 2007;318:944–949.
10. Joe MK, Sohn S, Hur W, Moon Y, Choi YR, Kee C. Accumulation of mutant myocilins in ER leads to ER stress and potential cytotoxicity in human trabecular meshwork cells. *Biochem Biophys Res Commun.* 2003;312:592–600.
11. Gould DB, Marchant JK, Savinova OV, Smith RS, John SW. Col4a1 mutation causes endoplasmic reticulum stress and genetically modifiable ocular dysgenesis. *Hum Mol Genet.* 2007;16:798–807.
12. Shimazawa M, Ito Y, Inokuchi Y, Hara H. Involvement of double-stranded RNA-dependent protein kinase in ER stress-induced retinal neuron damage. *Invest Ophthalmol Vis Sci.* 2007;48:3729–3736.
13. Shimazawa M, Inokuchi Y, Ito Y, et al. Involvement of ER stress in retinal cell death. *Mol Vis.* 2007;13:578–587.
14. Mahoney WC, Duksin D. Biological activities of the two major components of tunicamycin. *J Biol Chem.* 1979;254:6572–6576.
15. Awai M, Koga T, Inomata Y, et al. NMDA-induced retinal injury is mediated by an endoplasmic reticulum stress-related protein, CHOP/GADD153. *J Neurochem.* 2006;96:43–52.
16. Lee YK, Brewer JW, Hellman R, Hendershot LM. BiP and immunoglobulin light chain cooperate to control the folding of heavy chain and ensure the fidelity of immunoglobulin assembly. *Mol Biol Cell.* 1999;10:2209–2219.
17. Li WW, Alexandre S, Cao X, Lee AS. Transactivation of the grp78 promoter by Ca^{2+} depletion. A comparative analysis with A23187 and the endoplasmic reticulum Ca^{2+}-ATPase inhibitor thapsigargin. *J Biol Chem.* 1993;268:12003–12009.
18. van de Put FH, Elliott AC. The endoplasmic reticulum can act as a functional Ca^{2+} store in all subcellular regions of the pancreatic acinar cell. *J Biol Chem.* 1997;272:27764–27770.
19. Lievremont JP, Rizzuto R, Hendershot L, Meldolesi J. BiP, a major chaperone protein of the endoplasmic reticulum lumen, plays a direct and important role in the storage of the rapidly exchanging pool of Ca^{2+}. *J Biol Chem.* 1997;272:30873–30879.
20. Helenius A. How N-linked oligosaccharides affect glycoprotein folding in the endoplasmic reticulum. *Mol Biol Cell.* 1994;5:253–265.
21. Kuznetsov G, Chen LB, Nigam SK. Multiple molecular chaperones complex with misfolded large oligomeric glycoproteins in the endoplasmic reticulum. *J Biol Chem.* 1997;272:3057–3063.
22. Klausner RD, Sitia R. Protein degradation in the endoplasmic reticulum. *Cell.* 1990;62:611–614.
23. Blond-Elguindi S, Cwirla SE, Dower WJ, et al. Affinity panning of a library of peptides displayed on bacteriophages reveals the binding specificity of BiP. *Cell.* 1993;75:717–728.
24. Knarr G, Gething MJ, Modrow S, Buchner J. BiP binding sequences in antibodies. *J Biol Chem.* 1995;270:27589–27594.
25. Knarr G, Modrow S, Todd A, Gething MJ, Buchner J. BiP-binding sequences in HIV gp160. Implications for the binding specificity of bip. *J Biol Chem.* 1999;274:29850–29857.
26. Brodsky JL, Werner ED, Dubas ME, Goeckeler JL, Kruse KB, McCracken AA. The requirement for molecular chaperones during endoplasmic reticulum-associated protein degradation demonstrates that protein export and import are mechanistically distinct. *J Biol Chem.* 1999;274:3453–3460.
27. Meerovitch K, Wing S, Goltzman D. Proparathyroid hormone-related protein is associated with the chaperone protein BiP and undergoes proteasome-mediated degradation. *J Biol Chem.* 1998;273:21025–21030.
28. Katayama T, Imaizumi K, Sato N, et al. Presenilin-1 mutations downregulate the signalling pathway of the unfolded-protein response. *Nat Cell Biol.* 1999;1:479–485.
29. Yu Z, Luo H, Fu W, Mattson MP. The endoplasmic reticulum stress-responsive protein GRP78 protects neurons against excitotoxicity and apoptosis: suppression of oxidative stress and stabilization of calcium homeostasis. *Exp Neurol.* 1999;155:302–314.
30. Rao RV, Peel A, Logvinova A, et al. Coupling endoplasmic reticulum stress to the cell death program: role of the ER chaperone GRP78. *FEBS Lett.* 2002;514:122–128.
31. Reddy RK, Mao C, Baumeister P, Austin RC, Kaufman RJ, Lee AS. Endoplasmic reticulum chaperone protein GRP78 protects cells from apoptosis induced by topoisomerase inhibitors: role of ATP binding site in suppression of caspase-7 activation. *J Biol Chem.* 2003;278:20915–20924.
32. Kudo T, Kanemoto S, Hara H, et al. A molecular chaperone inducer protects neurons from ER stress. *Cell Death Differ.* 2008;15:364–375.
33. Krishnamoorthy RR, Agarwal P, Prasanna G, et al. Characterization of a transformed rat retinal ganglion cell line. *Brain Res Mol Brain Res.* 2001;86:1–12.
34. Chen D, Padiernos E, Ding F, Lossos IS, Lopez CD. Apoptosis-stimulating protein of p53-2 (ASPP2/53BP2L) is an E2F target gene. *Cell Death Differ.* 2005;12:358–368.
35. Jiang Y, Ahn EY, Ryu SH, et al. Cytotoxicity of psammaplin A from a two-sponge association may correlate with the inhibition of DNA replication. *BMC Cancer.* 2004;4:70.
36. Feng G, Mellor RH, Bernstein M, et al. Imaging neuronal subsets in transgenic mice expressing multiple spectral variants of GFP. *Neuron.* 2000;28:41–51.
37. Iwawaki T, Akai R, Kohno K, Miura M. A transgenic mouse model for monitoring endoplasmic reticulum stress. *Nat Med.* 2004;10:98–102.

38. Siliprandi R, Canella R, Carmignoto G, et al. N-methyl-D-aspartate-induced neurotoxicity in the adult rat retina. *Vis Neurosci.* 1992; 8:567–573.
39. Jeon CJ, Strettoi E, Masland RH. The major cell populations of the mouse retina. *J Neurosci.* 1998;18:8936–8946.
40. Onozuka T, Sawamura D, Goto M, Yokota K, Shimizu H. Possible role of endoplasmic reticulum stress in the pathogenesis of Darier's disease. *J Dermatol Sci.* 2006;41:217–220.
41. Weil M, Jacobson MD, Coles HS, et al. Constitutive expression of the machinery for programmed cell death. *J Cell Biol.* 1996;133: 1053–1059.
42. Taylor J, Gatchalian CL, Keen G, Rubin LL. Apoptosis in cerebellar granule neurones: involvement of interleukin-1 beta converting enzyme-like proteases. *J Neurochem.* 1997;68:1598–1605.
43. Inokuchi Y, Shimazawa M, Nakajima Y, Suemori S, Mishima S, Hara H. Brazilian green propolis protects against retinal damage in vitro and in vivo. *Evid Based Complement Alternat Med.* 2006;3:71–77.
44. Chidlow G, Wood JP, Manavis J, Osborne NN, Casson RJ. Expression of osteopontin in the rat retina: effects of excitotoxic and ischemic injuries. *Invest Ophthalmol Vis Sci.* 2008;49:762–771.
45. Sucher NJ, Lipton SA, Dreyer EB. Molecular basis of glutamate toxicity in retinal ganglion cells. *Vision Res.* 1997;37:3483–3493.
46. Henneberry RC, Novelli A, Cox JA, Lysko PG. Neurotoxicity at the N-methyl-D-aspartate receptor in energy-compromised neurons. An hypothesis for cell death in aging and disease. *Ann NY Acad Sci.* 1989;568:225–233.
47. Uehara T, Nakamura T, Yao D, et al. S-nitrosylated protein-disulphide isomerase links protein misfolding to neurodegeneration. *Nature.* 2006;441:513–517.
48. Wang XZ, Lawson B, Brewer JW, et al. Signals from the stressed endoplasmic reticulum induce C/EBP-homologous protein (CHOP/GADD153). *Mol Cell Biol.* 1996;16:4273–4280.
49. Ubeda M, Habener JF. CHOP gene expression in response to endoplasmic-reticular stress requires NFY interaction with different domains of a conserved DNA-binding element. *Nucleic Acids Res.* 2000;28:4987–4997.
50. Foti DM, Welihinda A, Kaufman RJ, Lee AS. Conservation and divergence of the yeast and mammalian unfolded protein response. Activation of specific mammalian endoplasmic reticulum stress element of the grp78/BiP promoter by yeast Hac1. *J Biol Chem.* 1999;274:30402–30409.

J Pharmacol Sci 109, 311 – 314 (2009)

Journal of Pharmacological Sciences

Short Communication

The Protective Effect of a Newly Developed Molecular Chaperone–Inducer Against Mouse Ischemic Acute Kidney Injury

Worapat Prachasilchai[1], Hiroko Sonoda[1], Naoko Yokota-Ikeda[2], Katsuaki Ito[1], Takashi Kudo[3], Kazunori Imaizumi[4], and Masahiro Ikeda[1,*]

[1]*Department of Veterinary Pharmacology, Faculty of Agriculture, University of Miyazaki, Miyazaki 889-2192, Japan*
[2]*Nephrology Division, Miyazaki Prefectural Miyazaki Hospital, Miyazaki 880-8510, Japan*
[3]*Psychiatry, Department of Integrated Medicine, Division of Internal Medicine, Osaka University Graduate School of Medicine, Suita 565-0871, Japan*
[4]*Division of Molecular and Cellular Biology, Department of Anatomy, Faculty of Medicine, University of Miyazaki, Miyazaki 889-1692, Japan*

Received October 6, 2008; Accepted December 1, 2008

Abstract. Activation of the unfolded protein response (UPR) has been suggested to attenuate renal ischemia-reperfusion (I/R) injury. We recently found a compound, namely BIX, that activated the UPR selectively through the activating transcription factor 6 pathway. This study examined the effect of BIX on renal I/R injury in mice. BIX selectively up-regulated renal BiP mRNA and protein. Pretreatment with BIX significantly ameliorated renal I/R injury. Co-administration of BIX and tunicamycin, a non-selective UPR inducer, provided no additional protection. Our results suggest that the UPR activation by BIX leads to a novel drug therapy against renal I/R injury.

Keywords: renal ischemia-reperfusion injury, endoplasmic reticulum (ER) stress, unfolded protein response

When protein folding in the endoplasmic reticulum (ER) is inhibited by hypoxia, multiple signal transduction pathways, namely the unfolded protein response (UPR), are triggered in order to deal with the unfolded proteins (1 – 3). Immunoglobulin binding protein (BiP) is a stress-inducible endoplasmic reticulum chaperone, which serves as a master modulator for the UPR network. BiP normally binds to and inhibits the activation of ER stress-sensor proteins such as PKR-like ER localized kinase (PERK), inositol-requiring transmembrane kinase and endonuclease (IRE) 1, and activating transcription factor (ATF) 6. When unfolded proteins accumulate, BiP dissociates from the ER stress-sensor proteins and the UPR is initiated through their activation. PERK phosphorylates eukaryotic initiation factor-2α (eIF2α) and the phosphorylated eIF2α inhibits protein translation, leading to the expression of C/EBP homologous protein (CHOP) that regulates ER stress–induced apoptosis. IRE1 converts X-box–binding protein (XBP)-1 pre-mRNA into mature mRNA, and the translated protein of the mature mRNA (XBP-1s) binds to its target sequence in the regulatory regions of chaperone genes to induce their transcription. Upon ER stress, ATF6 undergoes protein cleavage in the Golgi apparatus, and the resulting cytoplasmic portion of ATF6 acts as a transcription factor in the nucleus for a range of target genes including ER chaperone genes.

The mortality and morbidity associated with acute kidney injury (AKI) continue to be alarmingly high over three decades despite significant improvements in supportive care (4, 5). A major reason for this is a lack of specific drug therapy against AKI (4, 5).

Renal ischemia-reperfusion (I/R) injury is an important cause of AKI (4, 5). Several studies using UPR inducers, including tunicamycin, thapsigargin, and A23187 have indicated that the UPR is activated after renal I/R and that UPR activation reduces the severity of I/R-induced cell injury (6 – 8). Tunicamycin is known to accumulate unfolded proteins in the ER by inhibiting UDP-GlcNAc-dolichol phosphate GlcNAc-phosphate transferase, which

*Corresponding author. a0d302u@cc.miyazaki-u.ac.jp
Published online in J-STAGE on January 29, 2009 (in advance)
doi: 10.1254/jphs.08272SC

prevents N-glycosylation of proteins (3). Thapsigargin, a Ca^{2+}-pump inhibitor in the ER, and A23187, a Ca^{2+} ionophore, disrupt intracellular Ca^{2+} homeostasis (3). Since ER chaperone is known to require Ca^{2+}, these drugs affect proper protein folding, leading to the accumulation of unfolded proteins in the ER (3). Therefore when such drugs are administered to animals, the UPR is activated through all the ER stress-sensor protein pathways, including the PERK, IRE1, and ATF6 pathways.

Recently, while screening for compounds that induce the BiP transcript and protein, our group identified a small-molecule BiP inducer, 1-(3,4-dihydroxyohenyl)-2-thiocyanate-ethanone, which we named BiP inducer X (BIX) (9, 10). BIX markedly induces BiP mRNA and protein in cultured cells, preferentially mediated by the ATF6 pathway.

In order to identify potentially specific therapeutic targets against AKI, this study investigated the effect of a specific chemical UPR inducer, BIX, in a mouse model of renal I/R injury.

All animal studies were performed in accordance with the *Guide for the Care and Use of Laboratory Animals at the University of Miyazaki*. Male ddy mice (7-week-old) were purchased from Kyudo, Co. (Saga).

The renal I/R procedure was performed as described previously (11). Tunicamycin was purchased from Calbiochem (Darmstadt) and BIX was synthesized as described previously (9). Both drugs were dissolved in 30% DMSO + 70% saline. In the experiment shown in Fig. 1, both drugs were administered with a volume of 100 μl by sub renal capsule injection to minimize any indirect action under in vivo conditions (tunicamycin, 0.2 mg/kg; BIX, 2 mg/kg). In other experiments, both drugs were administered intraperitoneally to mice (tunicamycin, 1.5 mg/kg; BIX, 15 mg/kg). Based on the previous reports (8 – 10, 12), the regimen of drug administration has been optimized in a preliminary experiment. Plasma samples for the measurement of creatinine concentration were obtained at the indicated time points and then analyzed using an autoanalyzer (TBA-200FR; Toshiba Medical Systems Co., Ltd., Tokyo).

RT-PCR, immunoblotting, and histological analyses were performed as reported previously (8). Mouse BiP, XBP-1, CHOP, and glyceraldehyde 3-phosphate dehydrogenase (GAPDH) mRNA were amplified with the following primers: forward (5'-cacgtccaaccccgagaa-3') and reverse (5'-atgacccgctgatcaaagtc-3') for BiP, forward (5'-gaaccaggagttaagaacacg-3') and reverse (5'-aggcaacagtgtcagagtcc-3') for XBP-1, forward (5'-ctgcct ttcaccttggagac-3') and reverse (5'-ggacgcagggtcaagagtag-3') for CHOP, and forward (5'-aacgacccctcattgac-3') and reverse (5'-tccacgacatactcagcac-3') for GAPDH.

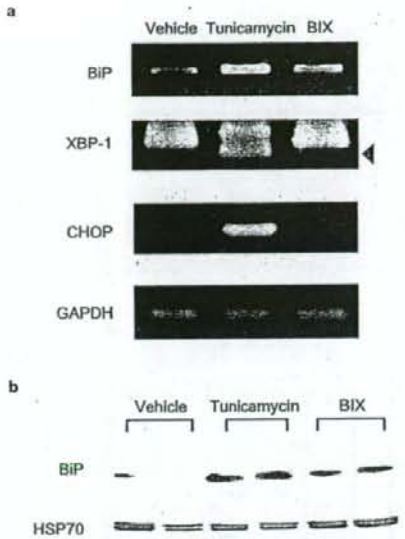

Fig. 1. XBP-1, BiP, CHOP mRNA, and BiP protein levels following BIX treatment. Mice were treated with vehicle, tunicamycin, or BIX for 12 h and then total RNA was extracted from whole kidney. a: BiP, a splicing form of XBP-1 mRNA (arrow head), and CHOP mRNA were determined by RT-PCR with the appropriate number of cycles. GAPDH mRNA was also examined as an internal control. b: At 24 h after treatment with the vehicle, tunicamycin, or BIX, protein was extracted from whole kidney. BiP and HSP70 proteins were detected by immunoblotting.

At 12 h after the treatment with BIX or tunicamycin, renal total RNA was extracted and analyzed by RT-PCR with a specific primer set for BiP, XBP-1, CHOP, or GAPDH. As shown in Fig. 1a, BIX up-regulated BiP mRNA but not XBP-1s, CHOP, and GAPDH mRNAs. This expression pattern was in accord with a previous report (9), indicating that BIX specifically acted on the ATF-6 pathway. In contrast, tunicamycin up-regulated all of BiP, XBP-1s, and CHOP mRNAs, indicating activation of the UPR through all the PERK, IRE1, and ATF6 pathways.

Next, we determined the expression level of BiP protein. After treatment with BIX or tunicamycin for 24 h, protein was extracted from mouse whole kidney and the extracted protein was subjected to immunoblotting. Figure 1b shows the representative blots. BiP protein was clearly increased by treatment with BIX or tunicamycin. The 70-kDa heat shock protein (HSP70) is a member of the same protein family as BiP and its expression is known to be unaltered in response to activation of the UPR (6, 8). We also examined the expression level of HSP70 after treatment with BIX or